Title: Ankyrin-1 gene exhibits allelic heterogeneity in conferring protection against malaria

Author list and affiliations

Hong Ming Huang[1], Denis C. Bauer[2], Patrick M. Lelliott[3], Matthew W. A. Dixon[4], Leann Tilley[4], Brendan J. McMorran[1], Simon J. Foote[1], Gaetan Burgio[1]*

[1] Department of Immunology and Infectious Disease, John Curtin School of Medical Research, Australian National University, ACT, Australia.

[2] CSIRO, Sydney, NSW, Australia.

[3] IFReC Research Building, Osaka University, 3-1 Yamada-oka, Suita, Osaka 565-0871, Japan.

[4] Department of Biochemistry and Molecular Biology, Bio21 Institute, Melbourne, Victoria, Australia.

Corresponding author*

Dr Gaetan Burgio

The John Curtin School of Medical Research, Australian National University,

131 Garran Road, ACT 2601, Australia.

Gaetan.burgio@anu.edu.au

+61 2 612 59428

Authors' Contributions

H.M.H., D.C.B., P.M.L., M.W.A.D, L.T., B.J.M, S.J.F. and G.B. designed and planned the experimental work. H.M.H., D.C.B. and G.B. performed the research. H.M.H., D.C.B., P.M.L., M.W.A.D, L.T., B.J.M, S.J.F. and G.B. interpreted and analysed the data. H.M.H., D.C.B. and G.B. performed statistical analysis. H.M.H, P.M.L., G.B., B.J.M. and S.J.F. wrote the manuscript. All authors reviewed the manuscript.

Abstract

Allelic heterogeneity is a common phenomenon where a gene exhibit different phenotype depending on the nature of genetic mutations. In the context of genes affecting malaria susceptibility, it allowed us to explore and understand the intricate host-parasite interactions during malaria infections. In this study, we described a gene encoding erythrocytic ankyrin-1 (*Ank-1*) which exhibit allelic heterogeneity during malaria infections. We employed ENU mutagenesis screen on mice and identified two *Ank-1* mutations, one resulted in an amino acid substitution (MRI95845), and the other a truncated *Ank-1* protein (MRI96570). Both mutations caused hereditary spherocytosis-like phenotypes and confer protection against *Plasmodium chabaudi* infections. Upon further examination, *Ank-1*$^{(MRI96570)}$ mutation was found to inhibit intra-erythrocytic parasite maturation, whereas *Ank-1*$^{(MRI95845)}$ caused increased bystander erythrocyte clearance during infection. This is the first description of allelic heterogeneity in ankyrin-1 from the direct comparison between two *Ank-1* mutations. Despite the lack of direct evidence from population studies, this observation further supported the protective roles of ankyrin-1 mutations in conferring malaria protection. This study also emphasised the importance of such phenomenon to achieve a better understanding of host-parasite interactions, which could be the basis of future studies.

Authors' summary

In malaria endemic regions, many individual developed natural resistance against the disease by having certain genetic mutations that affect the ability of malarial parasites to survive within the human body, notably the red blood cells. However, it is often observed that different mutations within the same gene could give rise to different degree of malaria protection. Through studying this phenomenon, we are able to better understand the underlying cause of their protective effects. In this report, we study two mutations of ankyrin-1 gene, MRI96570 and MRI95845, both of which protect mice from malaria infections. However, both of them exhibit stark differences in the way they mediate protection. MRI96570 affects the ability of malarial parasites to develop inside the red blood cells, whereas MRI95845 enhances the destruction of red blood cells during malaria infection. This is the first direct observation of two distinct methods of achieving malaria protection from ankyrin-1 gene. This report also highlights the complex relationship between the human and malarial parasites, and that such phenomenon might be more common than we initially expected.

Introduction

Historically, malarial parasites have been co-evolving with humans for thousands of years and have played a major role in shaping human genome in malaria endemic regions (1, 2). Indeed, many genetic polymorphisms were selected for as they provide significant survival advantages during malaria infections (1, 3), resulting in high frequencies of protective genetic mutations in malaria endemic regions. The majority of them affect the red blood cells (RBCs), and hence the blood stage of malaria infections (3-5).

Interestingly, these genetic mutations or alleles often exhibit varying degrees of malaria protection even if they affect the same gene, which is influenced by the location and the severity of mutations (6, 7). This phenomenon, known as “allelic heterogeneity”, is characterised by multiple different phenotypes arising from mutations in a single gene. It has been described for certain genes affecting malaria susceptibility, which is reflected by their geographical distribution within endemic regions (8). One of the most prominent examples of this is the G6PD deficiency disorder, which could arise from multiple mutations in G6PD gene (7, 9). Many studies have explored the effectiveness of each mutation in protecting individuals from malaria, which corresponds to the distribution of each allele across the globe (10-12). Another example is the β-globin gene, which is well known for its two malaria protective alleles – the HbS and HbC in African populations (13, 14). HbC is restricted to West Africa, whereas HbS is widespread throughout Africa, which is thought to be linked to the effectiveness of each allele to confer malaria resistance, and their associated morbidity (15, 16). Studies on these alleles would not only allow a better understanding of host-parasite interactions, but also give us insights into the dynamics of population genetics in malaria endemic regions (8).

However, allelic heterogeneity could also complicate the characterisation of the malaria protective roles of certain genes, often resulting in conflicting evidence from various studies. One example of such polymorphisms is CD36 deficiency, which was originally thought to be protective against malaria, as evidenced by the positive selection in East Asian and African populations (17-19). While

85 some studies reported increased malaria protection (20), others reported no significant associations
86 (21) or even increased susceptibility (17, 22). It is possible that these contradictive findings are due
87 to confounding factors associated with allelic heterogeneity in CD36 deficiency (6). This also further
88 emphasises the importance of taking allelic heterogeneity into consideration to enable a better
89 design in future studies involving host genetics in malaria, as well as various infectious diseases.

90 In contrast, the allelic heterogeneity of genes affecting RBC cytoskeleton in terms of malaria
91 susceptibility is poorly understood. Many of the resulting genetic disorders are heterogeneous, such
92 as hereditary spherocytosis (HS), which is characterised by the formation of "spherocytes", RBCs that
93 exhibit reduced volume due to disruptions in erythrocyte cytoskeletons. HS is caused by mutations
94 in ankyrin, spectrins, band 3 and protein 4.2, with ankyrin mutations contributing to more than 50%
95 of HS cases (23-27). HS also exhibits clinical heterogeneity, where the severity depends greatly on
96 the location and the nature of mutations (28). However, the prevalence of HS in malaria endemic
97 regions is not well studied, where only specific cases were reported (29-32). Nevertheless, *in vivo*
98 and *in vitro* studies have repeatedly suggested an association of HS with increased malaria resistance,
99 and several mechanisms have been proposed, although not all of them were consistent (33-36).
100 Based on these observations, we hypothesised that the inconsistencies in resistance mechanisms
101 might be due to the allelic heterogeneity of genes associated with HS.

102 To explore this hypothesis, we examined mouse models carrying two novel N-ethyl-N-nitrosourea
103 (ENU)-induced ankyrin mutations. These two mouse lines, *Ank-1*$^{(MRI96570/+)}$ and *Ank-1*$^{(MRI95845/MRI95845)}$,
104 displayed haematological and clinical features consistent with HS, and a marked resistance to
105 infection by the murine malarial parasite, *P. chabaudi*. Analysis of the underlying mechanism of
106 resistance to infection revealed both common and distinct features between the strains. RBCs from
107 both lines were similarly resistant to merozoite invasion. However, the *Ank-1*$^{(MRI95845/MRI95845)}$
108 erythrocytes were also more rapidly cleared from circulation during an infection, whereas an
109 impairment in intra-erythrocytic parasite maturation was observed in the infected *Ank-1*$^{(MRI96570/+)}$

110 erythrocytes. This study highlights the first direct examination of allelic heterogeneity of *Ank-1* gene
111 in the context of malaria resistance in mouse models.

112

113 **Results**

114 **MRI96570 and MRI95845 carry mutations in Ank-1 gene**

115 ENU-treated SJL/J male mice were crossed with wild-type female to produce G1 progeny. The G1
116 progeny carrying heterozygous point mutations in their genome were then subjected to
117 haematological screening to identify genes affecting RBC properties, as potential candidates that
118 might confer malaria protection. G1 mice MRI96570 and MRI95845 were identified from the ENU-
119 dominant screen with mean cellular volume (MCV) three standard deviations below the normal level
120 of the respective parental line - 48.5fl for MRI96570, and 50.6fl for MRI95845, compared to the
121 background of 55.1±1.2fl in SJL/J inbred strain. These mice were crossed with wild-type to produce
122 G2 progeny, where approximately half of them exhibit low erythrocyte MCV values. Two affected
123 MRI96570 and MRI95845 G2 progeny, which also showed a reduction of MCV, were sent for exome
124 sequencing to identify the causative genetic mutations. Unique variants shared between the
125 affected mice were filtered and selected for mice carrying MRI96570 mutation or MRI95845
126 mutation (S1 Table). A mutation in ankyrin-1 (*Ank-1*) gene was present in all the affected mice, and
127 co-segregated completely with the reduced MCV phenotype for over three generations of crosses.
128 Sanger sequencing revealed a T to A transversion in exon 34 of *Ank-1* gene for MRI96570 strain, and
129 a T to A transversion in exon 5 of *Ank-1* gene for MRI95845 strain (S1 Figure). They were predicted to
130 cause a nonsense mutation at amino acid position 1398, located in the spectrin-binding domain for
131 MRI96570 mice, and a substitution of tyrosine for asparagine at amino acid residue 149 in the 4th
132 ankyrin repeat for MRI95845 mice (Figure 1a). MRI96570 and MRI95845 will be referred as *Ank-*
133 $1^{(MRI96570)}$ and $Ank\text{-}1^{(MRI95845)}$ respectively, for the rest of the report.

Both *Ank-1*$^{(MRI96570)}$ and *Ank-1*$^{(MRI95845)}$ exhibit HS-like phenotypes

Since ankyrin mutations are usually associated with HS, we examined both *Ank-1*$^{(MRI96570)}$ and *Ank-1*$^{(MRI95845)}$ mice in terms of their HS-like phenotypes. When two *Ank-1*$^{(MRI96570/+)}$ G2 progeny were intercrossed, *Ank-1*$^{(MRI96570/MRI96570)}$ mice were born with severe jaundice and died within several days from birth (Figure 1b), suggesting homozygosity for *Ank-1*$^{(MRI96570)}$ mutation caused lethal anaemia. On the other hand, *Ank-1*$^{(MRI95845/MRI95845)}$ mice appeared healthy with normal lifespan. Haematological analysis of these mice revealed a significant reduction in MCV and mean corpuscular haemoglobin (MCH) and increased red cell distribution width (RDW) (S2 table), indicating microcytosis and anisocytosis, which are the hallmarks for HS. When the RBCs were subjected to osmotic stress, RBCs from *Ank-1*$^{(MRI96570/+)}$, *Ank-1*$^{(MRI95845/+)}$ and *Ank-1*$^{(MRI95845/MRI95845)}$ mice exhibit significantly increased RBC osmotic fragility compared to wild-type RBCs (Figure 1c). 50% haemolysis was observed at approximately 5.6 and 5.4 g/L (equivalent to 104mM and 100mM) sodium chloride, respectively, compared to approximately 4.6g/L (84mM) sodium chloride of wild-type. The *Ank-1*$^{(MRI95845/MRI95845)}$ RBCs showed further susceptibility towards osmotic stress, with 50% haemolysis at approximately 6.5 g/L (121mM) sodium chloride concentration.

We predicted that the mutant RBCs have shorter half-life, which is also one of the symptoms of HS. Therefore, RBC half-life was determined by biotinylating mouse RBCs and tracking the remaining biotinylated RBCs over time. As shown in Figure 1d, erythrocytes from *Ank-1*$^{(MRI95845/MRI95845)}$ RBCs have significantly shorter half-life of approximately 9.5 days as opposed to 16 days of wild-type erythrocytes, but no significant difference was observed for erythrocytes from heterozygous mice. The morphology of these RBCs were examined under light and scanning electron microscopy (S2 Figure). *Ank-1*$^{(MRI96570/+)}$ and *Ank-1*$^{(MRI95845/+)}$ mice exhibited slight reduction in RBC size, while *Ank-1*$^{(MRI95845/MRI95845)}$ mice had smaller RBCs and displayed anisocytosis and acanthocytic. On the other

158 hand, blood smears obtained from jaundiced *Ank-1*$^{(MRI96570/MRI96570)}$ pups showed reticulocytosis,
159 fragmented RBCs and severe anisocytosis.

160 Another feature of HS is the reduced RBC deformability, which was examined using two different
161 analytical techniques: ektacytometry and an *in vitro* spleen retention assay. Ektacytometry measures
162 the flexibility of RBCs when subjected to shear pressure, and expresses as an elongation index, which
163 indicates the deformability of RBCs. The *Ank-1*$^{(MRI96570/+)}$ RBCs showed reduced elongation index
164 compared to wild-type, whereas *Ank-1*$^{(MRI95845/MRI95845)}$ RBCs showed further reduction in elongation
165 index, indicating significant reduction in RBC deformability (Figure 1e). In addition, the *in vitro* spleen
166 retention assay was performed by passing the erythrocytes through layer of microbeads of varying
167 sizes, modelling *in vivo* splenic filtration. RBC deformability was assessed by the ability of RBCs to
168 pass through the bead layer. Figure 1f showed three independent measurements of RBC
169 deformability via splenic retention assay, comparing between wild-type, *Ank-1*$^{(MRI96570/+)}$, *Ank-*
170 *1*$^{(MRI95845/+)}$ and *Ank-1*$^{(MRI95845/MRI95845)}$ RBCs. An approximately 70% increased retention for *Ank-*
171 *1*$^{(MRI96570/+)}$ RBCs was observed compared to wild-type, whereas erythrocytes of *Ank-1*$^{(MRI95845/+)}$ and
172 *Ank-1*$^{(MRI95845/MRI95845)}$ mice showed 86% and 90% increased RBC retention compared to wild-type,
173 respectively. However, no significant difference was observed between *Ank-1*$^{(MRI96570/+)}$ and *Ank-*
174 *1*$^{(MRI95845/MRI95845)}$ erythrocytes.

175 The expression levels of ankyrin and other RBC membrane proteins were examined (S3 Figure).
176 Significant reduction of *Ank-1* mRNA levels was observed in *Ank-1*$^{(MRI96570/+)}$, *Ank-1*$^{(MRI95845/+)}$, *Ank-*
177 *1*$^{(MRI96570/MRI96570)}$ and *Ank-1*$^{(MRI95845/MRI95845)}$ embryonic livers (S3a Figure). However, coomassie staining
178 and Western blotting of the RBC membrane fractions did not show a significant difference in ANK-1
179 levels between wild-type, *Ank-1*$^{(MRI96570/+)}$ and *Ank-1*$^{(MRI95845/MRI95845)}$ erythrocytes (S3b-d Figure). The
180 predicted truncated ANK-1$^{(MRI96570/+)}$ form (160kDa) was also not evidenced. The levels of other
181 cytoskeletal proteins were also examined to account for possible disruptions to interactions with
182 other binding partners of ankyrin-1. However, no difference was observed for Band 3, α- and β-

183 spectrin, whereas significantly lower protein 4.2 level was observed in *Ank-1*$^{(MRI95845/MRI95845)}$
184 erythrocytes (S3d Figure).

185

186 **_Ank-1_$^{(MRI96570)}$ and _Ank-1_$^{(MRI95845)}$ confer protection against _P. chabaudi_ infection**

187 We proposed that mice carrying these mutations have reduced susceptibility to malaria infection,
188 which we examined by injecting with a lethal dose of *P. chabaudi*, and the percentage of parasitised
189 RBCs (parasitemia) was recorded. As shown in Figure 2a, *Ank-1*$^{(MRI96570/+)}$ and *Ank-1*$^{(MRI95845/+)}$ mice
190 showed significant reduction in peak parasitemia of approximately 15-20%, while *Ank-*
191 *1*$^{(MRI95845/MRI95845)}$ mice showed approximately 30% reduction in peak parasitemia compared to wild-
192 type. *Ank-1*$^{(MRI95845/MRI95845)}$ mice also showed a two-day delay in parasitemia, peaking on day 12 post-
193 infection rather than day 10 as with wild-type. *Ank-1*$^{(MRI95845/MRI95845)}$ mice also exhibited significantly
194 higher survival rate compared to wild-type during *P. chabaudi* infection, but no significant difference
195 was observed for *Ank-1*$^{(MRI96570/+)}$ and *Ank-1*$^{(MRI95845/+)}$ mice compared to wild-type (Figure 2b). Overall,
196 these results suggested that both *Ank-1*$^{(MRI96570/+)}$ and *Ank-1*$^{(MRI95845/+)}$ mice showed moderate
197 resistance, whereas *Ank-1*$^{(MRI95845/MRI95845)}$ mice exhibited significant resistance towards *P. chabaudi*
198 infection in relative to the wild-type mice.

199 From these results, we further investigated and compared the possible mechanisms of resistance
200 mediated by *Ank-1*$^{(MRI96570)}$ and *Ank-1*$^{(MRI95845)}$ mutations. We examined three important determinants
201 of parasite growth and survival within the host. Firstly, we studied the ability of parasite to survive
202 within these erythrocytes, since ankyrin-1 mutations have previously been implicated to impair
203 parasite intra-erythrocytic maturation (36). Secondly, the erythrocyte invasion was assessed as the
204 mutations disrupt erythrocyte cytoskeletal structure, which is important for facilitating efficient
205 erythrocyte invasion (37). Thirdly, the mutations might result in an improved detection of parasitised
206 RBCs, thus enhancing their removal from circulation during malaria infection. Since *Ank-1*$^{(MRI96570/+)}$

and *Ank-1*$^{(MRI95845/MRI95845)}$ mice exhibited differences in malaria resistance, we hypothesised that they mediate malaria resistance through different pathways.

Ank-1$^{(MRI96570/+)}$ **and** ***Ank-1***$^{(MRI95845/MRI95845)}$ **erythrocytes are resistant to merozoite invasion**

First, the ability of parasite to invade erythrocytes was assessed via an *in vivo* erythrocyte tracking (IVET) assay. Labelled RBCs from either wild-type, *Ank-1*$^{(MRI96570/+)}$ or *Ank-1*$^{(MRI95845/MRI95845)}$ mice were injected into infected wild-type mice of 1-10% parasitemia during late schizogony stage and the parasitemia of each genotype was monitored over 36-40 hours to indicate relative invasion rates. The initial invasion period was expected at 30 minutes to 3 hour timepoints, and the results were expressed as a ratio of parasitised RBCs of either, *Ank-1*$^{(MRI96570/+)}$ to wild-type (Figure 3a), *Ank-1*$^{(MRI95845/MRI95845)}$ to wild-type (Figure 3b), or *Ank-1*$^{(MRI96570/+)}$ to *Ank-1*$^{(MRI95845/MRI95845)}$ (Figure 3c). From Figure 3a and 3b, *Ank-1*$^{(MRI96570/+)}$ and *Ank-1*$^{(MRI95845/MRI95845)}$ erythrocytes were less parasitised compared to wild-type (0.6-0.7 for *Ank-1*$^{(MRI96570/+)}$ and 0.55-0.8 for *Ank-1*$^{(MRI95845/MRI95845)}$) from 3 hours up to 36 hours post-injection, indicating both *Ank-1*$^{(MRI96570/+)}$ and *Ank-1*$^{(MRI95845/MRI95845)}$ erythrocytes were more resistant to parasite invasion than wild-type. However, no significant differences in parasitemia ratio were observed at 30 minute timepoint. Furthermore, when the invasion rate of both *Ank-1*$^{(MRI96570/+)}$ and *Ank-1*$^{(MRI95845/MRI95845)}$ erythrocytes were compared in infected wild-type mice (Figure 3c), no significant difference in parasitemia ratio was observed, suggesting a similar invasion rate between the two mutant erythrocytes.

Ank-1$^{(MRI96570/+)}$ **erythrocytes impair parasite maturation**

Second, the parasite intra-erythrocytic maturation was determined through a TUNEL assay, which allows the detection of fragmented DNA in RBCs, as an indication of dying parasites (Figure 3d) (38). Samples were collected from infected mice at 1-10% parasitemia at both young ring stage and late

231 trophozoite stage, and the proportion of TUNEL-positive infected RBCs were calculated. As seen
232 from Figure 3e, more TUNEL-positive parasites were observed within *Ank-1*$^{(MRI96570/+)}$ erythrocytes, in
233 both ring (30.1±3.4% compared to 15.2±3.1% of wild-type) and trophozoite stage (30.8±3.8%
234 compared to 11.7±1.0% of wild-type), whereas no differences were observed for *Ank-1*$^{(MRI95845/+)}$ and
235 *Ank-1*$^{(MRI95845/MRI95845)}$ erythrocytes. This result suggested that the growth of parasites within *Ank-*
236 *1*$^{(MRI96570/+)}$ erythrocytes was impaired, but was normal in *Ank-1*$^{(MRI95845/+)}$ and *Ank-1*$^{(MRI95845/MRI95845)}$
237 erythrocytes. This also indicate that *Ank-1*$^{(MRI96570)}$ disrupts parasite maturation, whereas *Ank-*
238 *1*$^{(MRI95845)}$ seems to support normal parasite growth, although growth inhibition at other stages were
239 not studied.

240

241 ***Ank-1*$^{(MRI95845/MRI95845)}$ erythrocytes are more likely to get cleared during malaria infections, partially**
242 **via splenic filtration**

243 The proportions of labelled erythrocytes were also monitored during the IVET assays to compare the
244 relative loss of the two labelled RBC populations as the indicator of RBC clearance during malaria
245 infection. No significant reduction in *Ank-1*$^{(MRI96570/+)}$ erythrocyte numbers was observed during IVET
246 assay compared to wild-type (Figure 4a). On the other hand, the number of labelled *Ank-*
247 *1*$^{(MRI95845/MRI95845)}$ erythrocytes decreased significantly compared to wild-type and *Ank-1*$^{(MRI96570/+)}$
248 erythrocytes (Figure 4b and c), with approximately 20% and 50% reduction, respectively. However,
249 the parasitemia measurements during the IVET assays were approximately 2% to 16-30% (S4a-b
250 Figure), which did not correlate with the reduction of labelled *Ank-1*$^{(MRI95845/MRI95845)}$ erythrocytes.
251 This suggested an increased bystander clearance rather than clearance of infected *Ank-*
252 *1*$^{(MRI95845/MRI95845)}$ RBCs. To further verify this observation, the RBCs of infected mice from each
253 genotype were biotinylated and the RBC half-life was examined without blood transfusion. As shown
254 in Figure 4d, the *Ank-1*$^{(MRI96570/+)}$ mice exhibited no significant reduction in RBC numbers, whereas
255 *Ank-1*$^{(MRI95845/MRI95845)}$ mice were found to have significantly shorter half-life of approximately 6 days,

256 which did not correlate with the parasitemia curve (S4c Figure). This observation of shorter RBC half-
257 life in infected *Ank-1*$^{(MRI95845/MRI95845)}$ mice is consistent with the increased *Ank-1*$^{(MRI95845/MRI95845)}$
258 erythrocyte clearance as shown in IVET assays.

259 We proposed that the spleen played a major role in mediating this bystander clearance. Therefore,
260 we infected mice which had been splenectomised with *P. chabaudi* and infused with labelled wild-
261 type and *Ank-1*$^{(MRI95845/MRI95845)}$ erythrocytes, the proportions of which were monitored over time. As
262 shown in Figure 4e, *Ank-1*$^{(MRI95845/MRI95845)}$ erythrocyte numbers are approximately two-fold higher
263 ($P<0.01$) in splenectomised mice compared to non-splenectomised mice. This suggests that the
264 spleen is a major contributor towards *Ank-1*$^{(MRI95845/MRI95845)}$ erythrocyte clearance, although the
265 clearance was not completely abrogated in the absence of the spleen.

266

267 **Increased Band 3 mobility in *Ank-1*$^{(MRI95845/MRI95845)}$ erythrocytes as a likely mechanism for increased**
268 **clearance.**

269 Nevertheless, we hypothesised that this phenomenon is likely due to changes to the cytoskeletal
270 structure of *Ank-1*$^{(MRI95845/MRI95845)}$ RBCs. In order to support our hypothesis, we examined the band 3
271 mobility across the RBC membrane as an indicator of disrupted RBC cytoskeleton (39, 40). We
272 fluorescently labelled erythrocytic band 3 with eosin-5'-maleimide and performed Fluorescence
273 Recovery after Photobleaching (FRAP) on erythrocytes, which involved photobleaching with high-
274 powered laser followed by a recovery period where the fluorescence intensity was recorded. *Ank-*
275 *1*$^{(MRI95845/MRI95845)}$ RBCs were found to have significantly higher fluorescence recovery compared to
276 wild-type and *Ank-1*$^{(MRI96570/+)}$ RBCs (Figure 4f), which suggests a higher band 3 mobility in *Ank-*
277 *1*$^{(MRI95845/MRI95845)}$ erythrocytes, possibly due to an increased amount of band 3 that was not
278 associated with the RBC cytoskeleton.

279

Discussion

Ank-1 gene displayed allelic heterogeneity displayed allelic heterogeneity on host mice phenotypes and during malaria infections

Similar to HS in human populations, ankyrin mutations in mice also exhibit differences in clinical symptoms depending on the mutations. As shown in this study, homozygosity for MRI96570 mutation is lethal, while MRI95845 homozygotes appeared healthy, whereas both *Ank-1*$^{(MRI96570/+)}$ mice and *Ank-1*$^{(MRI95845/+)}$ mice exhibited HS-phenotypes with similar severity. While both mutations also conferred malaria protection and appeared to impair parasite invasion, they also showed some remarkable differences in mediating this resistance. Parasites in *Ank-1*$^{(MRI96570/+)}$ erythrocytes were more likely to be TUNEL-positive, indicating impaired intra-erythrocytic maturation, whereas *Ank-1*$^{(MRI95845/MRI95845)}$ erythrocytes were more likely to be removed from circulation and possibly increased turnover rate.

These findings were not exclusive to these two *Ank-1* mice described in this study. In fact, previous studies on other *Ank-1* mice also exhibit similar mechanisms of resistance. Notably, *Ank-1*$^{(MRI23420/+)}$ and *Ank-1*$^{(nb/nb)}$ mice were both reported to affect the parasite survival within the defective RBCs (33, 36). On the other hand, *Ank-1*$^{(MRI61689/+)}$ mice were also found to exhibit increased RBC bystander clearance (41), similar to *Ank-1*$^{(MRI95845/MRI95845)}$ mice. Nevertheless, this is the first direct report of such allelic heterogeneity described in *in vivo* mouse models, which highlighted the complexity behind the genetic resistance to malaria, especially in human populations.

Allelic heterogeneity of *Ank-1* and its association with malaria

However, due to lack of large scale studies on the HS prevalence in malaria endemic regions, ankyrin-1 has not been associated with malaria protection. Although HS prevalence is more well-characterised in Northern European and Japanese populations, with a prevalence of about 1 in 2000

(42-44), one study proposed an increased HS incidence in Algeria of about 1 in 1000 (45), raising the possibility of positive selection of HS by malarial parasites. However, as the result of extreme allelic heterogeneity of HS-causing genes, many alleles do not reach sufficient frequencies (46) or achieve consistent symptoms (47) to be easily associated with malaria protection. In addition, technical difficulties (29), confounding factors from large genetic variation in African populations (48), as well as poor diagnostics and health systems (48), pose significant challenges for dissecting the connection between HS and malaria. With development of more advanced technologies and better characterisation of the genetic structure of African populations, further studies into the association of HS and malaria could potentially yield beneficial insights into the co-evolutionary relationships between humans and *Plasmodium*.

Nonetheless, previous *in vivo* studies have indicated that *Ank*-1 mutations affect merozoite invasion and maturation (33, 36), both of which were also demonstrated in this study. However, this study also describes the first direct *in vivo* observation of different mutations in the *Ank-1* gene mediating two distinct, independent mechanisms of malaria resistance, where one impairs parasite maturation and the other increases RBC clearance. Ankyrin is one of the key proteins involved in RBC remodelling by parasites (49-51), and maintaining the structure of RBC cytoskeleton (28, 52). It is possible that this allelic heterogeneity is due to the effect each mutation has on the integrity of RBC cytoskeletal structure, as evidenced by the significantly increased band 3 mobility caused by *Ank-1*$^{(MRI95845)}$, but not *Ank-1*$^{(MRI96570)}$ mutation (Figure 4f). This suggests that mutations at different locations of the ankyrin-1 protein might have different effects on the RBCs, consequently impacts the ability of parasites to invade and grow. This hypothesis also agrees with the findings from other *Ank-1* mice from previous studies (35, 36, 41), where each mutation exhibited differences in terms of mechanisms of malaria resistance, which could be the basis for further studies.

Similarities of allelic heterogeneity in *Ank-1* and other malaria susceptibility genes

As evidenced from this study, the protective effect of the *Ank-1* gene against malaria is dependent on the nature and the location of mutations within the gene. Similarly, this allelic heterogeneity is also observed in other malaria susceptibility genes in human populations. For instance, although many G6PD deficiency-causing alleles have been implicated with malaria protection (53, 54), the protective effects are often debated, with many studies reporting increased, or no protection, for individuals with certain alleles of G6PD deficiency (55-60). This is thought to be due to the phenotypic complexity of G6PD deficiency associated with malaria susceptibility (7). Indeed, various G6PD alleles have been shown to cause a reduction of G6PD activity with differing severity, and was proposed to correlate with the malaria protection they conferred (55). More recently, Clarke and colleagues proposed reduced G6PD activity is associated with lower risk of cerebral malaria, but in exchange for higher risk of malaria anaemia (12), suggesting a delicate balance underlying the high frequency of G6PD polymorphism in populations of malaria endemic region. Similarly, *Ank-1* mutations described in this study, as well as other previous mouse studies (33, 35, 36), exhibit variability in malaria resistance, most likely as the result of allelic heterogeneity.

The heterogeneity in malaria resistance mechanisms of the *Ank-1* gene as observed in this study is comparable to the two prevalent alleles of the β-globin gene – the HbS and HbC, which result from amino acid substitution at position 6 from glutamate to valine, or lysine, respectively. They exhibit some similarities in mediating malaria resistance, including impaired parasite growth (61, 62), reduced cytoadherence (63-65) and increased erythrocyte clearance (66). However, HbS erythrocytes were found to be more resistant to all forms of malaria, whereas HbC erythrocytes appeared to be protective against cerebral malaria (15). This difference in malaria protection was proposed to correlate with distribution of HbS and HbC in Africa (16), further emphasising the importance of allelic heterogeneity in understanding host-parasite interactions.

In conclusion, we reported a novel observation where the *Ank-1* gene exhibits phenotypic heterogeneity in mediating malaria resistance mechanisms either via impairing intra-erythrocytic

parasite growth, or promoting RBC clearance. This study also highlighted that the allelic heterogeneity in relation to malaria resistance is not exclusive to G6PD deficiency, and it could also be much more common than we expected. Further studies should extend the understanding of the effects of various *Ank-1* mutations on the development of intra-erythrocytic parasites, as well as the association of HS with malaria in human populations. This could provide new insights into the intricate relationships between RBC cytoskeletal structure and parasite interactions.

Materials and Methods

Mice and ethics statement

All mice used in this study were housed with 12 hour light-dark cycle under constant temperature at 21 °C. All procedures were performed according to the National Health and Medical Research Council (NHMRC) Australian code of practice. Experiments were carried out under ethics agreement AEEC A2014/54, which was approved by the animal ethics committees of the Australian National University.

ENU mutagenesis and dominant phenotype screening

SJL/J male mice were injected intraperitoneally with two dose of 100 mg/kg ENU (Sigma-Aldrich, St Louis, MO) at one week interval. The treated males (G0) were crossed to females from the isogenic background to produce the first generation progeny (G1). The seven-week-old G1 progeny were bled and analysed on an Advia 120 Automated Haematology Analyser (Siemens, Berlin, Germany) to identify abnormal red blood cell count. Mouse carrying MRI96570 or MRI95845 mutation was identified with a “mean corpuscular volume” (MCV) value three standard deviations lower from other G1 progeny. It was crossed with SJL/J mice to produce G2 progeny to test the heritability of

the mutations and the dominance mode of inheritance. Mice that exhibited low MCV (<48fL) were selected for whole exome sequencing and genotyping.

Whole exome sequencing

DNA from two G2 mice carrying the abnormal red blood cell parameters (MCV <48fL) were extracted with Qiagen DNeasy blood and tissue kit (Qiagen, Venlo, Netherlands) for exome sequencing as previous described (67). Briefly, 10µg of DNA was prepared for exome enrichment with Agilent Sure select kit paired-end genomic library from Illumina (San Diego, CA), followed by high throughput sequencing using a HiSeq 2000 platform. The bioinformatics analysis was conducted according to the variant filtering method previously described by Bauer, McMorran (68). Private variants that were shared between the two mutants but not with other SJL/J, C57BL/6 mice or previously described ENU mutants were annotated using ANNOVAR (69). Private non-synonymous exonic and intronic variants within 20 bp from the exon spicing sites were retained as potential candidate ENU mutations.

PCR and Sanger sequencing

DNA from mutant mice were amplified through PCR with 35 cycles of 30 seconds of 95^0C denaturation, 30 seconds of 56-58^0C annealing and 72^0C elongation for 40 seconds. The primers used in the PCR are described as below. The PCR products were examined with agarose gel electrophoresis before being sent to the Australian Genome Research Facility (AGRF) in Melbourne, Australia, for Sanger sequencing. Logarithm of odds (LOD) score was calculated based on the number of mice that segregated with the candidate mutations.

Primers for MRI95845 mutation:

Amplicon	Forward	Reverse

Snai2	CATCTGCAGACCCACTCTGA	TGGTTGGTAAGCACATGAGAA
Tbc1d23	CACCCCCTTTTTGGTTTCTT	ACGTGCACATCGACTAACCA
Pnpla6	AGGCTGAGGAAGTGTGCCTA	AACTAGCTGGGCTTTGGTCA
Zglp1	CTGGCCTTTGACTTCTGACC	CCTCACAAGGTGGCTGTTTC
Ank-1	CTCCAAGTGAGAGGGTTTGC	GATGGCACACAGTCAGACCA

Primers for MRI96570 mutation:

Amplicon	Forward	Reverse
Fat4	CGCATCCCTTCATACAACCT	ACACCCCACTCACGTAGCTC
Rhcg	TGAGGAATGAGGGAGAAAGG	CCAATATGGCAGCCCTCTAA
Plxnb3	TACCCGATCAATCCAGAAGG	TTCTGAATGTGCAGGGTCAC
Ank-1	TGTGCAGGCATTTCTACATGA	ACTCTCTGGGTAGACCCCGT

RBC osmotic fragility analysis

To assess the susceptibility of RBC membrane to osmotic stress, 5µl of mouse whole blood was diluted 100-fold with phosphate buffer (pH 7.4) containing 0 to 10g/L of sodium chloride, and incubated for at least 10 minutes at room temperature. The cells were centrifuged at 800g for 3 minutes, and the supernatant, which contains free haemoglobin, was measured at 540nm to assess the degree of haemolysis. The absorbance values were expressed as percentage of haemolysis, with haemolysis at 0g/L sodium considered as 100% lysis.

Erythrocyte lifetime assay

Each uninfected mouse was injected with 1mg of EZ-link® Sulfo-NHS- LC Biotin (Biotin) (Thermo Scientific, Waltham, MA) in MT-PBS intravenously. 2ul of blood was collected on day 1, 7, 14, 21 and 28 from the day of injection. Samples were stained and analysed using a flow cytometer (details described in method 2.4.5). The proportion of Biotin-labelled mature RBCs on day 1 was considered as the “starting point” of 100% of labelled cells. For subsequent timepoints, the remaining number

of biotin-labelled RBCs were expressed as a percentage of the starting number as the indication of RBC turnover rate.

For infected mice, 1mg of Biotin was injected intravenously as soon as parasitemia was detectable on flow cytometry (approximately 0.05-0.3%). Samples were collected daily and analysed as above.

Ektacytometry

10-15ul of uninfected RBCs were first resuspended in 500ul of pre-warmed polyvinylpyrrolidone (PVP) solution at a viscosity of 30 mPa/second at 37 °C until needed. Samples were analyzed according to the manufacturer's instructions with a RheoScan Ektacytometer (Rheo Meditech, Seoul, South Korea) and the elongation index measured across a range of pressures from 0-20 Pa. Each sample was measured three times to account for technical variabilities. The values were normalized against the wild-type samples.

In vitro spleen retention assay

The RBC deformability were examined according to the protocol described previous by Deplaine, Safeukui (70) with modifications. Briefly, RBCs from each genotype of mice were stained with 10µg/ml of either hydroxysulfosuccinimide Atto 633 (Atto 633) or hydroxysulfosuccinimide Atto 565 (Atto 565) (Sigma-Aldrich, St Louis, MO), followed by three washes with MTRC (154mM NaCl, 5.6mM KCl, 1mM $MgCl_2$, 2.2mM $CaCl_2$, 20mM HEPES, 10mM glucose, 4mM EDTA, 0.5% BSA, pH 7.4, filter sterilized). The stained RBCs were mixed in equal proportion and diluted with unstained wild-type RBCs to give approximately 10-20% of the total RBCs being labelled RBCs. The samples were further diluted to 1-2% haematocrit with MTRC, before passing through the filter bed. The pre-filtered and post-filtered samples were analysed on BD LSRFortessa (BD Biosciences, Franklin Lakes, NJ) flow cytometer to determine the proportion being retained in the filter bed.

443

444 *Scanning electron microscopy (SEM)*

445 SEM was performed as described previously (41). Mouse blood was fixed overnight in 3% EM-grade
446 glutaraldehyde (Sigma-Aldrich, St Louis, MO) at 4°C immediately upon collection. The samples were
447 washed with MT-PBS 3 times, 10 minute each time. The cells were then adhered to the coverslips
448 with 0.1% polyethylenimine (PEI) for 10 minutes, before washing with MT-PBS. The cells were then
449 dried serially using 30%, 50%, 70%, 80%, 90%, 100%, 100% ethanol, 10 minutes each time. The cells
450 were then soaked in 1:1 ethanol: hexamethyldisilazane solution for 10 minutes, followed by 2
451 washes with 100% hexamethyldisilazane (Sigma-Aldrich, St Louis, MO), each 10 minutes. The
452 coverslips were then air-dried overnight and coated with gold and examined under JEOL JSM-6480LV
453 scanning electron microscope.

454

455 *Quantitative PCR and cDNA sequencing*

456 RNA was purified from embryonic livers of E14 embryos using Qiagen RNeasy kit (Qiagen, Venlo,
457 Netherlands), followed by cDNA synthesis using Transcriptor High Fidelity cDNA Synthesis Kit (Roche,
458 Basel, Switzerland), as described previously (41). Quantitative PCR was performed on ViiA™ 7 Real-
459 Time PCR System (Thermo Scientific, Waltham, MA). The $\Delta\Delta C_T$ method (71) was used to determine
460 the cDNA levels of *Ank-1* and the housekeeping gene β-actin and expressed as a fold-change of the
461 mutants to the wild-type. The primers used for *Ank-1* gene spanned exon 2 to 4: *Ank-1*-F: 5'-
462 TAACCAGAACGGGTTGAACG-3'; *Ank-1*-R: 5'-TGTTCCCCTTCTTGGTTGTC-3'; β-Actin-F: 5'-
463 TTCTTTGCAGCTCCTTCGTTGCCG-3'; β-Actin-R: 5'- TGGATGCGTACGTACATGGCTGGG-3'.

464

465 *SDS-PAGE, Coomassie staining and Western blot*

466 The analysis of erythrocytic proteins was carried out as described previously (41). Briefly, RBC ghosts
467 were prepared by lysing mouse RBCs with ice-cold 5mM phosphate buffer (ph7.4) and centrifuged at
468 20,000g for 20 minutes followed by removal of the supernatant, and repeat until the supernatant
469 became clear. The RBC ghosts or whole blood lysates were denatured in SDS-PAGE loading buffer
470 (0.0625M Tris pH 6.8, 2% SDS, 10% glycerol, 0.1M DTT, 0.01% bromophenol blue) at 95°C for 5
471 minutes before loading onto a Mini-PROTEAN® TGX™ Precast Gels (Bio-Rad, Hercules, CA). The gels
472 were then either stained with Coomassie blue solution (45% v/v methanol, 7% v/v acetic acid, 0.25%
473 w/v Brilliant Blue G) overnight or transferred to a nitrocellulose membrane. The western blot was
474 carried out using these primary antibodies: anti-alpha 1 spectrin (clone 17C7), anti-beta 1 spectrin
475 (clone 4C3) (Abcam, Cambridge, UK), anti-GAPDH (clone 6C5) (Merck Millipore, Darmstadt,
476 Germany), anti-N-terminal *Ank-1* "p89", anti-Band 3 and anti-protein 4.2 (kind gifts from Connie
477 Birkenmeier, Jackson Laboratory, US). Each primary antibody was detected with the appropriate
478 horseradish peroxidase (HRP)-conjugated secondary antibody at 1:5000 dilution from 1mg/ml stocks.
479 The blots were visualised using ImageQuant LAS 4000 (GE Healthcare Life Sciences, Arlington Heights,
480 IL), and quantified using ImageJ software (72).

481

482 *Malaria infection*

483 Malaria infections on mice were performed as described previously (41). 200µl of thawed *P.*
484 *chabaudi adami* infected blood was injected into the intraperitoneal cavity of a C57BL/6 donor
485 mouse. When the donor mouse reached 1-10% parasite load (parasitemia), blood was collected
486 through cardiac puncture. The blood was diluted with Krebs' buffered saline with 0.2% glucose as
487 described previously (73). Each experimental mouse was infected with $1x10^4$ parasites
488 intraperitoneally. The parasitemia of these mice were monitored either using light microscopy or
489 flow cytometry.

490

491 *Terminal deoxynucleotidyl transferase dUTP nick end labelling (TUNEL) staining*

492 The TUNEL assay was carried out as described previously (41) with slight modification. 3µl of
493 infected blood containing 1-10% parasitemia were collected during trophozoite stage and fixed in 1
494 in 4 diluted BD Cytofix™ Fixation Buffer (BD Biosciences, Franklin Lakes, NJ) for at least day until they
495 were needed. Each sample was then washed twice with MT-PBS, and adhered to a glass slide pre-
496 coated with 0.1% polyethylenimine (PEI) for 10 minutes at room temperature. The excess cells were
497 washed and incubated overnight at room temperature with TUNEL labelling solution (1mM Cobalt
498 Chloride, 25mM Tris-HCl pH 6.6, 200mM sodium cacodylate, 0.25mg/ml BSA, 60uM BrdUTP, 15U
499 Terminal transferase). The slides were washed three times, followed by staining with 50µg/ml of
500 anti-BrdU-FITC antibody (Novus Biologicals, Littleton, CO) in MT-PBT (MT-PBS, 0.5% BSA, 0.05%
501 Triton X-100) for 1 hour. The slides were then washed three times with MT-PBS and mounted with
502 SlowFade® Gold antifade reagent with DAPI (Thermo Scientific, Waltham, MA) and sealed. When the
503 slides were dried, they were examined using Axioplan 2 fluorescence light microscope (Carl Zeiss,
504 Oberkochen, Germany) between 600x to 1000x magnification. At least 100 DAPI-positive cells were
505 counted, and each was graded as either positive or negative for TUNEL staining, as an indication of
506 DNA fragmentation.

507

508 *In vivo erythrocyte tracking (IVET) assays*

509 The IVET assay was carried out as previously described by Lelliott, Lampkin (74), (75). Briefly, at least
510 1.5ml whole blood was collected from mice of each genotype via cardiac puncture, followed by
511 staining with either 10µg/ml of Atto 633 or 125µg/ml of EZ-Link™ Sulfo-NHS-LC-Biotin (Biotin)
512 (Thermo Scientific, Waltham, MA) for 45 minutes at room temperature, followed by washing two
513 times with MT-PBS. The blood was mixed in two different dye combinations to correct for any dye
514 effects. Approximately $1x10^9$ erythrocytes were injected intravenously into infected wild-type mice
515 at 1-5% parasitemia during schizogony stage. Blood samples were collected at various timepoints,

516 from 30 minutes up to 36 hours after injection, and analysed using flow cytometry. The ratio of
517 infected labelled erythrocytes was determined, as an indication of the relative susceptibility of RBCs
518 to *P. chabaudi* infections. The proportion of labelled blood populations was also tracked over time to
519 determine the clearance of these RBCs from the circulation.

520

521 *Flow cytometry analysis of blood samples*

522 For erythrocyte lifetime assays, 2µl of whole blood samples were stained with 2µg/ml streptavidin-
523 PE-Cy7, 1µg/ml anti-CD71-allophycocyanin (APC) (clone R17217), 1µg/ml anti-CD45–APC eFluor 780
524 (clone 30-F11) (eBioscience, San Diego, CA), 4µM Hoechst 33342 (Sigma-Aldrich, St Louis, MO) and
525 12µM JC-1 (Thermo Scientific, Waltham, MA) in MTRC. The samples were washed once with MTRC
526 and further stained with 2µg/ml streptavidin-PE-Cy7 to capture all biotin-labelled cells. Immediately
527 prior to analysing on flow cytometer, 5µl of 123count eBeads (eBioscience, San Diego, CA) was
528 added to determine the relative anaemic levels.

529 For both malaria infections and IVET assay, 2µl of whole blood samples were stained with 2µg/ml
530 streptavidin-PE-Cy7 (only for experiments with biotinylated erythrocytes), 1µg/ml anti-CD45–
531 allophycocyanin (APC)–eFluor 780 (clone 30-F11), 1µg/ml anti-CD71 (TFR1)–PerCP–eFluor 710 (clone
532 R17217) (eBioscience, San Diego, CA), 4µM Hoechst 33342 (Sigma-Aldrich, St Louis, MO) and 12µM
533 JC-1 (Thermo Scientific, Waltham, MA) in MTRC. All samples analysed through flow cytometry were
534 performed on BD LSRFortessa (BD Biosciences, Franklin Lakes, NJ), where 200,000 to 1,000,000
535 events were collected and visualized on FACSDiva^{TM} and FlowJo software. RBCs were identified by
536 gating on CD71 negative and CD45 negative population, followed by gating on Atto-labelled and
537 Biotin-labelled erythrocytes on appropriate channels (APC for Atto-633, PE for Atto-565 and PE-Cy7
538 for Biotin). The parasitemia of each labelled erythrocyte population was determined by gating on
539 Hoechst 33342 positive and JC-1 positive population.

Statistical analysis

The statistical analysis was carried out as described in previous study (41). The LOD score method coupled with Bonferroni correction was used to determine the causative mutation for MRI96570 and MRI95845. The statistical significance of the malaria survival was tested using the Log-Rank test. The statistical significance of parasite infection was determined via the statmod software package for R (http://bioinf.wehi.edu.au/software/compareCurves) using the 'compareGrowthCurves' function with 10,000 permutation, followed by adjustments for multiple testing. The statistical significance for the ratios of IVET assays was determined using the one sample t-test with hypothetical mean of 1. For the rest of the results, statistical significance was determined using two-tailed Students t-tests.

Acknowledgement

We would like to acknowledge Shelley Lampkin and Australian Phenomics Facility (APF) for the maintenance of the mouse colonies. We are also grateful for the assistance of the Microscopy Unit of the Macquarie University in the sample preparation and operation of the scanning electron microscope. This study was funded from the National Health and Medical Research Council (NHMRC) of Australia (Program Grant 490037, and Project Grants 605524 and APP1047090), the National Collaborative Research Infrastructure Strategy (NCRIS), the Education Investment Fund from the Department of Education and Training, the Australian Phenomics Network,

Literature Cited:

1. Kwiatkowski DP. How malaria has affected the human genome and what human genetics can teach us about malaria. Am J Hum Genet. 2005;77(2):171-92.
2. Hedrick PW. Resistance to malaria in humans: the impact of strong, recent selection. Malaria Journal. 2012;11(1):349.
3. Williams TN. Red blood cell defects and malaria. Mol Biochem Parasitol. 2006;149(2):121-7.
4. Williams TN. Human red blood cell polymorphisms and malaria. Curr Opin Microbiol. 2006;9(4):388-94.
5. Lell B, May J, Schmidt-Ott RJ, Lehman LG, Luckner D, Greve B, et al. The role of red blood cell polymorphisms in resistance and susceptibility to malaria. Clinical infectious diseases : an official publication of the Infectious Diseases Society of America. 1999;28(4):794-9.
6. Fry AE, Ghansa A, Small KS, Palma A, Auburn S, Diakite M, et al. Positive selection of a CD36 nonsense variant in sub-Saharan Africa, but no association with severe malaria phenotypes. Hum Mol Genet. 2009;18(14):2683-92.
7. Clark T, Fry A, Auburn S, Campino S, Diakite M, Green A. Allelic heterogeneity of G6PD deficiency in West Africa and severe malaria susceptibility. Eur J Hum Genet. 2009;17.
8. Bauduer F. Red cell polymorphisms and malaria: an evolutionary approach. Bulletins et mémoires de la Société d'anthropologie de Paris. 2013;25(1):55-64.
9. Beutler E, Kuhl W, Sáenz GF, Rodríguez W. Mutation analysis of glucose-6-phosphate dehydrogenase (G6PD) variants in Costa Rica. Hum Genet. 1991;87.
10. Howes RE, Battle KE, Satyagraha AW, Baird JK, Hay SI. G6PD deficiency: Global distribution, genetic variants and primaquine therapy. Adv Parasitol. 2013;81.
11. Shah SS, Rockett KA, Jallow M, Sisay-Joof F, Bojang KA, Pinder M, et al. Heterogeneous alleles comprising G6PD deficiency trait in West Africa exert contrasting effects on two major clinical presentations of severe malaria. Malaria Journal. 2016;15(1):1-8.
12. Clarke GM, Rockett K, Kivinen K, Hubbart C, Jeffreys AE, Rowlands K, et al. Characterisation of the opposing effects of G6PD deficiency on cerebral malaria and severe malarial anaemia. eLife. 2017;6:e15085.
13. Kilian N, Srismith S, Dittmer M, Ouermi D, Bisseye C, Simpore J, et al. Hemoglobin S and C affect protein export in Plasmodium falciparum-infected erythrocytes. Biology Open. 2015;4(3):400-10.
14. May J, Evans JA, Timmann C, Ehmen C, Busch W, Thye T, et al. Hemoglobin variants and disease manifestations in severe falciparum malaria. Jama. 2007;297(20):2220-6.
15. Kreuels B, Kreuzberg C, Kobbe R, Ayim-Akonor M, Apiah-Thompson P, Thompson B, et al. Differing effects of HbS and HbC traits on uncomplicated falciparum malaria, anemia, and child growth. Blood. 2010;115(22):4551-8.
16. Gonçalves BP, Gupta S, Penman BS. Sickle haemoglobin, haemoglobin C and malaria mortality feedbacks. Malaria Journal. 2016;15(1):26.
17. Aitman TJ, Cooper LD, Norsworthy PJ, Wahid FN, Gray JK, Curtis BR, et al. Malaria susceptibility and CD36 mutation. Nature. 2000;405(6790):1015-6.
18. Curtis BR, Aster RH. Incidence of the Nak(a)-negative platelet phenotype in African Americans is similar to that of Asians. Transfusion. 1996;36(4):331-4.
19. Urwijitaroon Y, Barusrux S, Romphruk A, Puapairoj C. Frequency of human platelet antigens among blood donors in northeastern Thailand. Transfusion. 1995;35(10):868-70.
20. Pain A, Urban BC, Kai O, Casals-Pascual C, Shafi J, Marsh K, et al. A non-sense mutation in Cd36 gene is associated with protection from severe malaria. Lancet. 2001;357(9267):1502-3.
21. Amodu OK, Gbadegesin RA, Ralph SA, Adeyemo AA, Brenchley PE, Ayoola OO, et al. Plasmodium falciparum malaria in south-west Nigerian children: is the polymorphism of ICAM-1 and E-selectin genes contributing to the clinical severity of malaria? Acta tropica. 2005;95(3):248-55.

612 22. Ayodo G, Price AL, Keinan A, Ajwang A, Otieno MF, Orago AS, et al. Combining evidence of
613 natural selection with association analysis increases power to detect malaria-resistance variants. Am
614 J Hum Genet. 2007;81(2):234-42.
615 23. Gallagher PG, Forget BG. Hematologically Important Mutations: Spectrin and Ankyrin
616 Variants in Hereditary Spherocytosis. Blood Cells, Molecules, and Diseases. 1998;24(4):539-43.
617 24. Jarolim P, Murray JL, Rubin HL, Taylor WM, Prchal JT, Ballas SK, et al. Characterization of 13
618 novel band 3 gene defects in hereditary spherocytosis with band 3 deficiency. Blood.
619 1996;88(11):4366-74.
620 25. Takaoka Y, Ideguchi H, Matsuda M, Sakamoto N, Takeuchi T, Fukumaki Y. A novel mutation
621 in the erythrocyte protein 4.2 gene of Japanese patients with hereditary spherocytosis (protein 4.2
622 Fukuoka). Br J Haematol. 1994;88(3):527-33.
623 26. Matsuda M, Hatano N, Ideguchi H, Takahira H, Fukumaki Y. A novel mutation causing an
624 aberrant splicing in the protein 4.2 gene associated with hereditary spherocytosis (protein
625 4.2Notame). Hum Mol Genet. 1995;4(7):1187-91.
626 27. Eber SW, Gonzalez JM, Lux ML, Scarpa AL, Tse WT, Dornwell M, et al. Ankyrin-1 mutations
627 are a major cause of dominant and recessive hereditary spherocytosis. Nat Genet. 1996;13(2):214-8.
628 28. Gallagher PG. Hematologically important mutations: ankyrin variants in hereditary
629 spherocytosis. Blood Cells Mol Dis. 2005;35(3):345-7.
630 29. Sangerman J, Maksimova Y, Edelman EJ, Morrow JS, Forget BG, Gallagher PG. Ankyrin-linked
631 hereditary spherocytosis in an African-American kindred. Am J Hematol. 2008;83(10):789-94.
632 30. Spector I, Metz J. A Bantu family with hereditary spherocytosis. S Afr Med J. 1963;37:211-3.
633 31. Hassan A, Babadoko AA, Isa AH, Abunimye P. Hereditary spherocytosis in a 27-year-old
634 woman: case report. Annals of African medicine. 2009;8(1):61-3.
635 32. Ustun C, Kutlar F, Holley L, Seigler M, Burgess R, Kutlar A. Interaction of sickle cell trait with
636 hereditary spherocytosis: splenic infarcts and sequestration. Acta Haematol. 2003;109(1):46-9.
637 33. Shear HL, Roth EF, Jr., Ng C, Nagel RL. Resistance to malaria in ankyrin and spectrin deficient
638 mice. Br J Haematol. 1991;78(4):555-60.
639 34. Schulman S, Roth EF, Jr., Cheng B, Rybicki AC, Sussman, II, Wong M, et al. Growth of
640 Plasmodium falciparum in human erythrocytes containing abnormal membrane proteins. Proc Natl
641 Acad Sci U S A. 1990;87(18):7339-43.
642 35. Rank G, Sutton R, Marshall V, Lundie RJ, Caddy J, Romeo T, et al. Novel roles for erythroid
643 Ankyrin-1 revealed through an ENU-induced null mouse mutant. Blood. 2009;113(14):3352-62.
644 36. Greth A, Lampkin S, Mayura-Guru P, Rodda F, Drysdale K, Roberts-Thomson M, et al. A novel
645 ENU-mutation in ankyrin-1 disrupts malaria parasite maturation in red blood cells of mice. PLoS One.
646 2012;7(6):e38999.
647 37. Chishti AH, Palek J, Fisher D, Maalouf GJ, Liu SC. Reduced invasion and growth of
648 Plasmodium falciparum into elliptocytic red blood cells with a combined deficiency of protein 4.1,
649 glycophorin C, and p55. Blood. 1996;87(8):3462-9.
650 38. McMorran BJ, Marshall VM, de Graaf C, Drysdale KE, Shabbar M, Smyth GK, et al. Platelets
651 Kill Intraerythrocytic Malarial Parasites and Mediate Survival to Infection. Science.
652 2009;323(5915):797-800.
653 39. Kodippili GC, Spector J, Sullivan C, Kuypers FA, Labotka R, Gallagher PG, et al. Imaging of the
654 diffusion of single band 3 molecules on normal and mutant erythrocytes. Blood. 2009;113(24):6237-
655 45.
656 40. Cho MR, Eber SW, Liu S-C, Lux SE, Golan DE. Regulation of Band 3 Rotational Mobility by
657 Ankyrin in Intact Human Red Cells. Biochemistry. 1998;37(51):17828-35.
658 41. Huang HM, Bauer DC, Lelliott PM, Greth A, McMorran BJ, Foote SJ, et al. A novel ENU-
659 induced ankyrin-1 mutation impairs parasite invasion and increases erythrocyte clearance during
660 malaria infection in mice. Scientific reports. 2016;6:37197.
661 42. Godal HC, Heisto H. High prevalence of increased osmotic fragility of red blood cells among
662 Norwegian blood donors. Scandinavian journal of haematology. 1981;27(1):30-4.

663 43. Eber SW, Pekrun A, Neufeldt A, Schroter W. Prevalence of increased osmotic fragility of
664 erythrocytes in German blood donors: screening using a modified glycerol lysis test. Annals of
665 hematology. 1992;64(2):88-92.
666 44. Yawata Y, Kanzaki A, Yawata A, Doerfler W, Ozcan R, Eber SW. Characteristic features of the
667 genotype and phenotype of hereditary spherocytosis in the Japanese population. Int J Hematol.
668 2000;71(2):118-35.
669 45. Zerhouni F, Guetarni D, Henni T, Colonna P. Occurrence and characteristics of hereditary
670 spherocytosis in Algeria. European journal of haematology. 1991;47(1):42-7.
671 46. Kavallaris M, Ng D, Byrne F. Cytoskeleton and Human Disease: Springer; 2012.
672 47. Shah S, Vega R. Hereditary Spherocytosis. Pediatrics in Review. 2004;25(5):168-72.
673 48. A global network for investigating the genomic epidemiology of malaria. Nature.
674 2008;456(7223):732-7.
675 49. Maier AG, Cooke BM, Cowman AF, Tilley L. Malaria parasite proteins that remodel the host
676 erythrocyte. Nat Rev Micro. 2009;7(5):341-54.
677 50. Zuccala ES, Baum J. Cytoskeletal and membrane remodelling during malaria parasite
678 invasion of the human erythrocyte. Br J Haematol. 2011;154(6):680-9.
679 51. Hanspal M, Dua M, Takakuwa Y, Chishti AH, Mizuno A. Plasmodium falciparum cysteine
680 protease falcipain-2 cleaves erythrocyte membrane skeletal proteins at late stages of parasite
681 development. Presented in part in abstract form at the 43rd Annual Meeting of the American Society
682 of Hematology, Orlando, FL, 2001. 2002;100(3):1048-54.
683 52. Miraglia del Giudice E, Iolascon A, Pinto L, Nobili B, Perrotta S. Erythrocyte membrane
684 protein alterations underlying clinical heterogeneity in hereditary spherocytosis. Br J Haematol.
685 1994;88(1):52-5.
686 53. Ruwende C, Hill A. Glucose-6-phosphate dehydrogenase deficiency and malaria. Journal of
687 molecular medicine (Berlin, Germany). 1998;76(8):581-8.
688 54. Mason PJ, Bautista JM, Gilsanz F. G6PD deficiency: the genotype-phenotype association.
689 Blood Rev. 2007;21.
690 55. Manjurano A, Sepulveda N, Nadjm B, Mtove G, Wangai H, Maxwell C. African glucose-6-
691 phosphate dehydrogenase alleles associated with protection from severe malaria in heterozygous
692 females in Tanzania. PLoS Genet. 2015;11.
693 56. Ruwende C, Khoo SC, Snow RW, Yates SN, Kwiatkowski D, Gupta S. Natural selection of
694 hemi- and heterozygotes for G6PD deficiency in Africa by resistance to severe malaria. Nature.
695 1995;376.
696 57. Guindo A, Fairhurst RM, Doumbo OK, Wellems TE, Diallo DA. X-Linked G6PD Deficiency
697 Protects Hemizygous Males but Not Heterozygous Females against Severe Malaria. PLoS Medicine.
698 2007;4(3):e66.
699 58. Sirugo G, Predazzi IM, Bartlett J, Tacconelli A, Walther M, Williams SM. G6PD A- deficiency
700 and severe malaria in The Gambia: heterozygote advantage and possible homozygote disadvantage.
701 Am J Trop Med Hyg. 2014;90.
702 59. Toure O, Konate S, Sissoko S, Niangaly A, Barry A, Sall AH, et al. Candidate polymorphisms
703 and severe malaria in a Malian population. PLoS One. 2012;7(9):e43987.
704 60. Martin SK, Miller LH, Alling D, Okoye VC, Esan GJ, Osunkoya BO. Severe malaria and glucose-
705 6-phosphate-dehydrogenase deficiency: a reappraisal of the malaria/G-6-P.D. hypothesis. Lancet.
706 1979;1.
707 61. Fairhurst RM, Fujioka H, Hayton K, Collins KF, Wellems TE. Aberrant development of
708 Plasmodium falciparum in hemoglobin CC red cells: implications for the malaria protective effect of
709 the homozygous state. Blood. 2003;101(8):3309-15.
710 62. Cyrklaff M, Sanchez CP, Kilian N, Bisseye C, Simpore J, Frischknecht F, et al. Hemoglobins S
711 and C interfere with actin remodeling in Plasmodium falciparum-infected erythrocytes. Science.
712 2011;334(6060):1283-6.

63. Carlson J, Nash GB, Gabutti V, al Yaman F, Wahlgren M. Natural protection against severe Plasmodium falciparum malaria due to impaired rosette formation. Blood. 1994;84.
64. Fairhurst RM, Bess CD, Krause MA. Abnormal PfEMP1/knob display on Plasmodium falciparum-infected erythrocytes containing hemoglobin variants: fresh insights into malaria pathogenesis and protection. Microbes and Infection / Institut Pasteur. 2012;14(10):851-62.
65. Fairhurst RM, Baruch DI, Brittain NJ, Ostera GR, Wallach JS, Hoang HL, et al. Abnormal display of PfEMP-1 on erythrocytes carrying haemoglobin C may protect against malaria. Nature. 2005;435(7045):1117-21.
66. Ayi K, Turrini F, Piga A, Arese P. Enhanced phagocytosis of ring-parasitized mutant erythrocytes: a common mechanism that may explain protection against falciparum malaria in sickle trait and beta-thalassemia trait. Blood. 2004;104(10):3364-71.
67. Hortle E, Nijagal B, Bauer DC, Jensen LM, Ahn SB, Cockburn IA, et al. Adenosine monophosphate deaminase 3 activation shortens erythrocyte half-life and provides malaria resistance in mice. Blood. 2016.
68. Bauer DC, McMorran BJ, Foote SJ, Burgio G. Genome-wide analysis of chemically induced mutations in mouse in phenotype-driven screens. BMC Genomics. 2015;16(1):1-8.
69. Wang K, Li M, Hakonarson H. ANNOVAR: functional annotation of genetic variants from high-throughput sequencing data. Nucleic Acids Research. 2010;38(16):e164-e.
70. Deplaine G, Safeukui I, Jeddi F, Lacoste F, Brousse V, Perrot S, et al. The sensing of poorly deformable red blood cells by the human spleen can be mimicked in vitro. Blood. 2011;117(8):e88-95.
71. Livak KJ, Schmittgen TD. Analysis of relative gene expression data using real-time quantitative PCR and the 2− ΔΔCT method. methods. 2001;25(4):402-8.
72. Schneider CA, Rasband WS, Eliceiri KW. NIH Image to ImageJ: 25 years of image analysis. Nat Meth. 2012;9(7):671-5.
73. Jarra W, Brown K. Protective immunity to malaria: studies with cloned lines of Plasmodium chabaudi and P. berghei in CBA/Ca mice. I. The effectiveness and inter - and intra - species specificity of immunity induced by infection. Parasite immunology. 1985;7(6):595-606.
74. Lelliott PM, Lampkin S, McMorran BJ, Foote SJ, Burgio G. A flow cytometric assay to quantify invasion of red blood cells by rodent Plasmodium parasites in vivo. Malar J. 2014;13:100.
75. Lelliott PM, McMorran BJ, Foote SJ, Burgio G. In vivo assessment of rodent Plasmodium parasitemia and merozoite invasion by flow cytometry. JoVE (Journal of Visualized Experiments). 2015(98):e52736-e.

753 **Figure Captions**

754 **Figure 1. The mutations and phenotypes of *Ank-1*$^{(MRI96570/+)}$, *Ank-1*$^{(MRI95845/+)}$ and *Ank-1*$^{(MRI95845/MRI95845)}$**
755 **mice.** The location of ankyrin-1 mutations in *Ank-1*$^{(MRI96570)}$ and *Ank-1*$^{(MRI95845)}$ alleles and the
756 predicted effects on ankyrin-1 protein (a). The *Ank-1*$^{(MRI96570/MRI96570)}$ pups (indicated by arrows)
757 showed severe jaundice and died within 1 week after birth (b). The osmotic fragility of *Ank-*
758 *1*$^{(MRI96570/+)}$, *Ank-1*$^{(MRI95845/+)}$ and *Ank-1*$^{(MRI95845/MRI95845)}$ erythrocytes in hypotonic solution from 0-10g/L
759 sodium (n=5) (c). The RBC half-life of *Ank-1*$^{(MRI96570/+)}$, *Ank-1*$^{(MRI95845/+)}$ and *Ank-1*$^{(MRI95845/MRI95845)}$ mice
760 (n=5) (d). The elasticity of *Ank-1*$^{(MRI96570/+)}$ and *Ank-1*$^{(MRI95845/MRI95845)}$ RBCs under shear pressure as
761 measured by ektacytometer (n=3) (e). The proportion of retained *Ank-1*$^{(MRI96570/+)}$, *Ank-1*$^{(MRI95845/+)}$ and
762 *Ank-1*$^{(MRI95845/MRI95845)}$ RBCs when passing through a layer of beads during the *in vitro* spleen retention
763 assay (n=3) (f). * P<0.05, ** P<0.01, *** P<0.001. All error bars indicate standard error of mean
764 (SEM).

765

766 **Figure 2. The parasitemia and survival curve of *Ank-1*$^{(MRI96570/+)}$, *Ank-1*$^{(MRI95845/+)}$ and *Ank-**
767 ***1*$^{(MRI95845/MRI95845)}$ mice when challenged with *P. chabaudi*.** The parasite load (a) and survival rate (b)
768 of *Ank-1*$^{(MRI96570/+)}$, *Ank-1*$^{(MRI95845/+)}$ and *Ank-1*$^{(MRI95845/MRI95845)}$ mice from day 7 to day 15 post-infection
769 when challenged with $1x10^4$ parasite intraperitoneally as determined by light microscopy. (n=9-13).
770 * P<0.05, *** P<0.001. Error bars indicate SEM.

771

772 **Figure 3. The parasite invasion and intra-erythrocytic growth as indicated via IVET and TUNEL**
773 **assay.** The relative invasion efficiency into *Ank-1*$^{(MRI96570/+)}$ and *Ank-1*$^{(MRI95845/MRI95845)}$ erythrocytes was
774 examined through IVET assay, where parasitemia ratio was calculated from parasite load of either
775 *Ank-1*$^{(MRI96570/+)}$ to wild-type (a), *Ank-1*$^{(MRI95845/MRI95845)}$ to wild-type (b), or *Ank-1*$^{(MRI96570/+)}$ to *Ank-*
776 *1*$^{(MRI95845/MRI95845)}$ erythrocytes (c) (n=5-7). The parasite growth inhibition was determined via TUNEL

777 assay on infected RBCs (DAPI-positive) as an indicator of apoptotic and necrotic parasites (d). The
778 proportion of TUNEL-positive infected RBCs was counted for *Ank-1*$^{(MRI96570/+)}$, *Ank-1*$^{(MRI95845/+)}$ and
779 *Ank-1*$^{(MRI95845/MRI95845)}$ mice at 1-5% parasitemia at ring stage (6-8 hours) and late trophozoite (18-20
780 hours) stage (n=4)(e). *P<0.05, **P<0.01, ***P<0.001. Error bars indicates SEM.

781

782 **Figure 4. The clearance of wild-type, *Ank-1*$^{(MRI96570/+)}$ *Ank-1*$^{(MRI95845/MRI95845)}$ erythrocytes during**
783 **malaria infection and the mobility of erythrocytic Band 3.** The remaining percentage of labelled
784 RBCs was monitored during the course of IVET assays, comparing between wild-type and *Ank-*
785 *1*$^{(MRI96570/+)}$ erythrocytes (a), wild-type and *Ank-1*$^{(MRI95845/MRI95845)}$ erythrocytes (b), and *Ank-1*$^{(MRI96570/+)}$
786 and *Ank-1*$^{(MRI95845/MRI95845)}$ erythrocytes (c) (n=5-7). The half-life of wild-type, *Ank-1*$^{(MRI96570/+)}$ *Ank-*
787 *1*$^{(MRI95845/MRI95845)}$ erythrocytes during malaria infection as determined by biotinylation of RBCs when
788 parasites were detectable (n=6-7) (d). The clearance of wild-type and *Ank-1*$^{(MRI95845/MRI95845)}$
789 erythrocytes in splenectomised and non-splenectomised mice infected with *P. chabaudi* over 3 days
790 starting from 1% parasitemia (n=6) (e). The band 3 mobility on RBC membrane was measured using
791 Fluorescence recovery after Photobleaching (FRAP), showing the recovery rate of fluorescence as a
792 result of Band 3 migration to the bleach spot (n=9-21) (f). ** P<0.01, *** P<0.001. Error bars indicate
793 SEM.

794

795

796 **Supporting Information Captions**

797 **S1 Figure. The location of *Ank-1*$^{(MRI96570)}$ and *Ank-1*$^{(MRI95845)}$ mutation.** Sanger sequencing of mice
798 carrying *Ank-1*$^{(MRI96570)}$ revealed a T to A transversion in exon 34 of *Ank-1* gene, which is predicted to
799 induce a premature stop codon (a). Mice carrying *Ank-1*$^{(MRI95845)}$ mutation were found to have a T to

800 A transversion in exon 5 of *Ank-1* gene, which is predicted to cause a missense mutation from
801 tyrosine to asparagine at residue 149 (b).

802

803 **S2 Figure. The RBC morphology of mice carrying *Ank-1*$^{(MRI96570)}$ or *Ank-1*$^{(MRI95845)}$ mutation.** Giemsa-
804 stained blood smears as examined under light microscope at 1000x magnification (a). Scanning
805 electron microscopic images showing the RBC shape of *Ank-1*$^{(MRI96570/+)}$, *Ank-1*$^{(MRI95845/+)}$ and *Ank-*
806 *1*$^{(MRI95845/MRI95845)}$ mice (b).

807

808 **S3 Figure. The expression of *Ank-1* and other RBC cytoskeletal proteins in mice carrying *Ank-***
809 ***1*$^{(MRI96570)}$ or *Ank-1*$^{(MRI95845)}$ mutation.** Quantitative PCR was carried out on E14 embryonic livers to
810 examine *Ank-1* expression levels (n=3) (a). The abundance of ANK-1 and other RBC cytoskeletal
811 protein levels of of *Ank-1*$^{(MRI96570/+)}$, *Ank-1*$^{(MRI95845/+)}$ and *Ank-1*$^{(MRI95845/MRI95845)}$ mice as examined via
812 Coomassie (b) and Western blot (c) on membrane of mature RBCs. The relative abundance of
813 various cytoskeletal protein levels calculated from western blots (n=3) (d). SPTA = α-spectrin, SPTB =
814 β-spectrin, P 4.2 = Protein 4.2. * P<0.05, ** P<0.01. Error bars indicate SEM.

815

816 **S4 Figure. The parasitemia of the host mice during IVET assays and half-life assay.** The parasitemia
817 curve of the host mice during IVET assays, when comparing wild-type with *Ank-1*$^{(MRI95845/MRI95845)}$
818 erythrocytes (a), and *Ank-1*$^{(MRI96570/+)}$ with *Ank-1*$^{(MRI95845/MRI95845)}$ erythrocytes (b) (n=5-7). The
819 parasitemia curve of wild-type, *Ank-1*$^{(MRI96570/+)}$ and *Ank-1*$^{(MRI95845/MRI95845)}$ mice during RBC half-life
820 assay (n=6-7) (c).

821

822 **S1 Table. The candidate genes for MRI96570 and MRI95845 mutations.**

823 Variants from exome sequencing were filtered to exclude strain-specific variants and variants found
824 in other ENU-induced mice. Variants that were shared between the two mice carrying MRI96570
825 mutation or MRI95845 mutation are shown in (a) and (b), respectively. For each mutation, the
826 candidate genes were Sanger sequenced in affected mice to determine the correlation between the
827 genetic mutations and the phenotype by calculating the LOD score. LOD Threshold = 1.9 for
828 MRI96570, 2.0 for MRI95845 (n= 10).

829

830 **S2 Table. The complete blood count of *Ank-1*$^{(MRI96570/+)}$, *Ank-1*$^{(MRI95845/+)}$ and *Ank-1*$^{(MRI95845/MRI95845)}$**
831 **mice.**

832 The blood parameters were obtained from a haematological analyser ADVIA 120. WBC = white blood
833 cell count; RBC = red blood cell count; HGB = total haemoglobin; MCV = mean corpuscular volume;
834 MCH = mean corpuscular haemoglobin; MCHC = mean corpuscular haemoglobin concentration;
835 RDW = red cell distribution width; PLT = platelet counts; Retics = percentage of reticulocytes, n=23-
836 50. Bonferroni adjusted significance threshold = 0.001852, * P< 0.001, ** P< $1x10^{-5}$ compared to
837 wild-type mice; whereas ^ P<0.001 compared to *Ank-1*$^{(MRI95845/+)}$ mice.

838

Figure 1

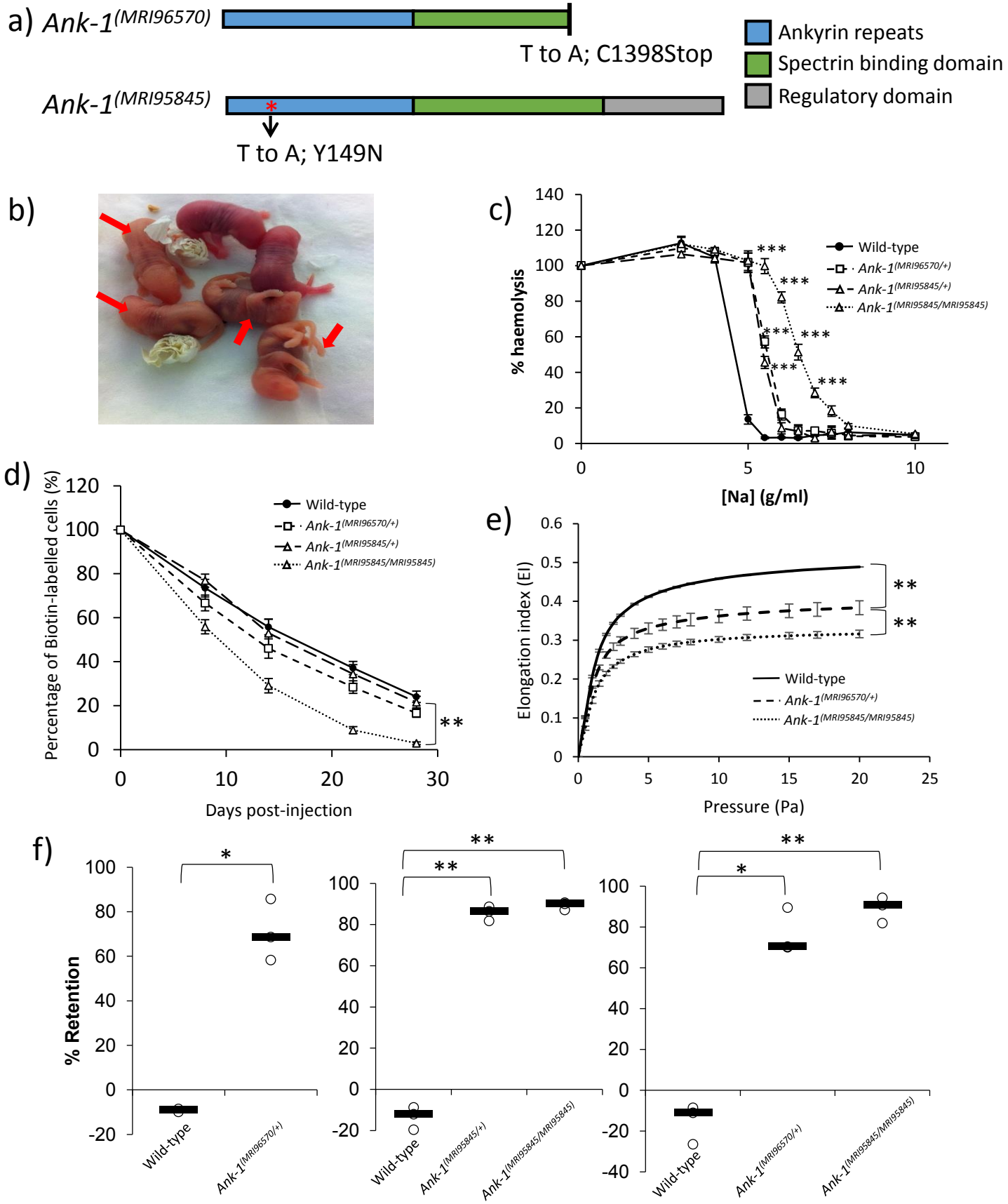

Figure 1. The mutations and phenotypes of *Ank-1*$^{(MRI96570/+)}$, *Ank-1*$^{(MRI95845/+)}$ and *Ank-1*$^{(MRI95845/MRI95845)}$ mice. The location of ankyrin-1 mutations in *Ank-1*$^{(MRI96570)}$ and *Ank-1*$^{(MRI95845)}$ alleles and the predicted effects on ankyrin-1 protein (a). The *Ank-1*$^{(MRI96570/MRI96570)}$ pups (indicated by arrows) showed severe jaundice and died within 1 week after birth (b). The osmotic fragility of *Ank-1*$^{(MRI96570/+)}$, *Ank-1*$^{(MRI95845/+)}$ and *Ank-1*$^{(MRI95845/MRI95845)}$ erythrocytes in hypotonic solution from 0-10g/L sodium (n=5) (c). The RBC half-life of *Ank-1*$^{(MRI96570/+)}$, *Ank-1*$^{(MRI95845/+)}$ and *Ank-1*$^{(MRI95845/MRI95845)}$ mice (n=5) (d). The elasticity of *Ank-1*$^{(MRI96570/+)}$ and *Ank-1*$^{(MRI95845/MRI95845)}$ RBCs under shear pressure as measured by ektacytometer (n=3) (e). The proportion of retained *Ank-1*$^{(MRI96570/+)}$, *Ank-1*$^{(MRI95845/+)}$ and *Ank-1*$^{(MRI95845/MRI95845)}$ RBCs when passing through a layer of beads during the *in vitro* spleen retention assay (n=3) (f). * P<0.05, ** P<0.01, *** P<0.001. All error bars indicate standard error of mean (SEM).

Figure 2

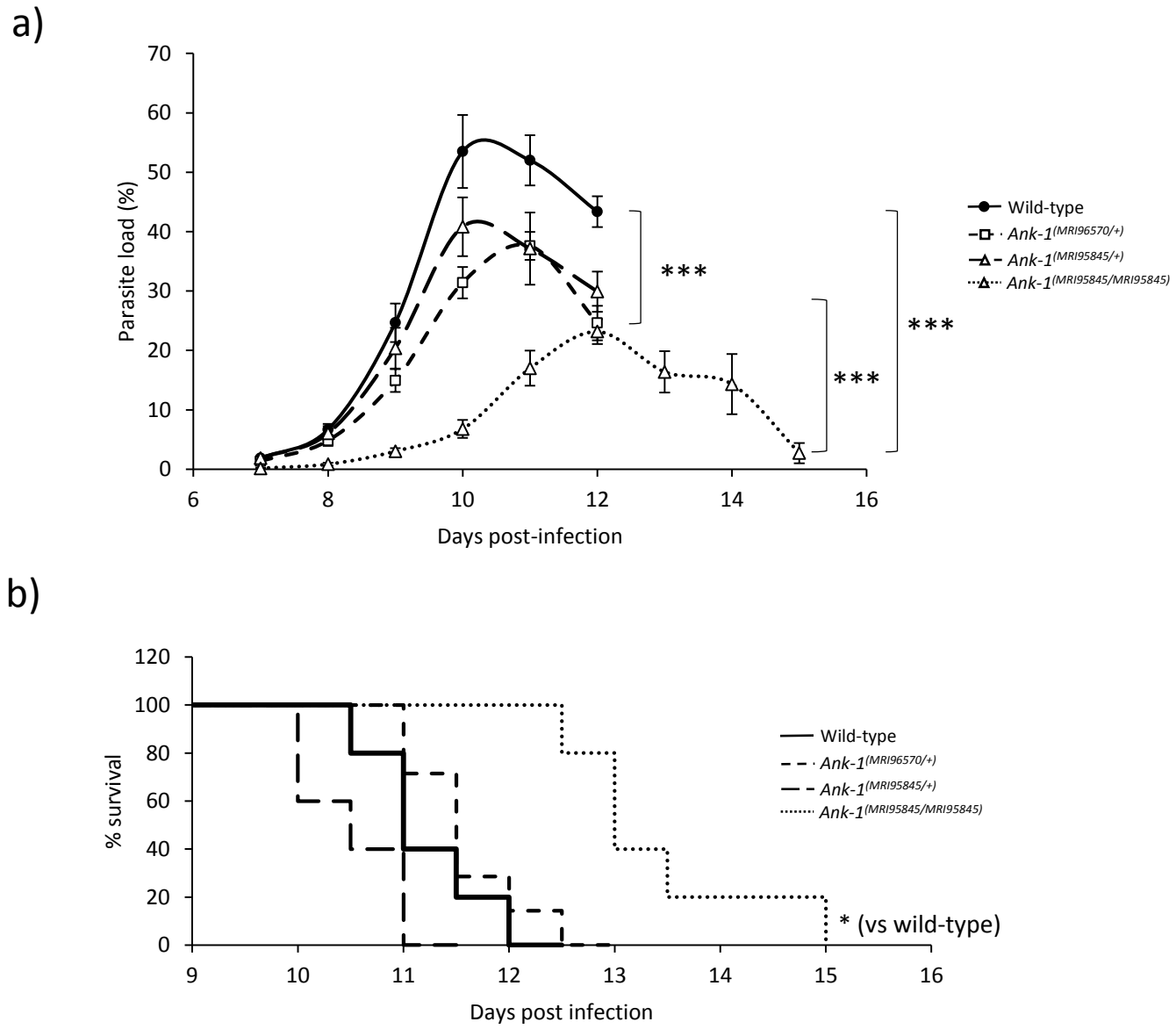

Figure 2. The parasitaemia and survival curve of *Ank-1*$^{(MRI96570/+)}$, *Ank-1*$^{(MRI95845/+)}$ and *Ank-1*$^{(MRI95845/MRI95845)}$ mice when challenged with *P. chabaudi*. The parasite load (a) and survival rate (b) of *Ank-1*$^{(MRI96570/+)}$, *Ank-1*$^{(MRI95845/+)}$ and *Ank-1*$^{(MRI95845/MRI95845)}$ mice from day 7 to day 15 post-infection when challenged with 1x10^4 parasite intraperitoneally as determined by light microscopy. (n=9-13). * P<0.05, *** P<0.001. Error bars indicate SEM.

Figure 3

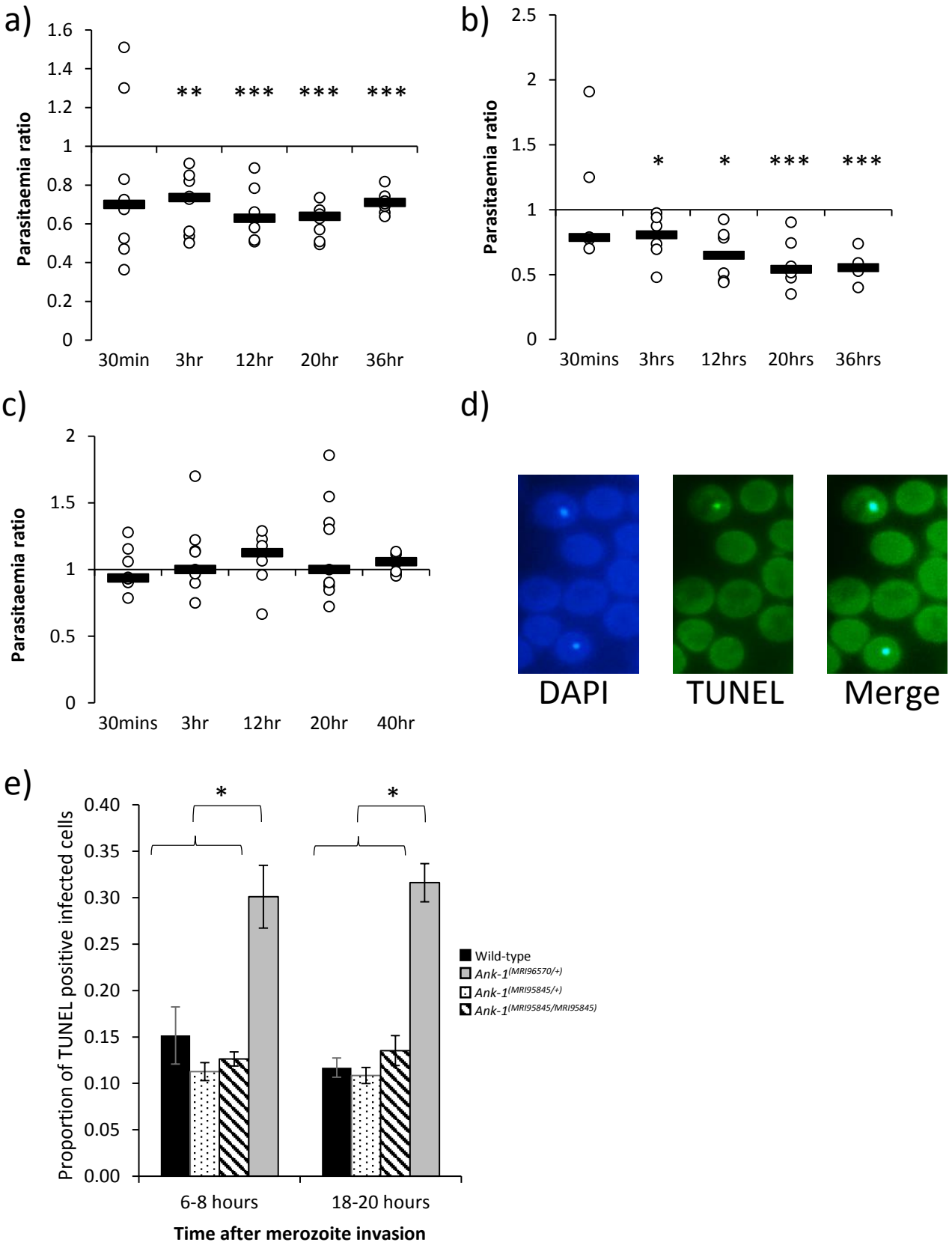

Figure 3. The parasite invasion and intra-erythrocytic growth as indicated via IVET and TUNEL assay. The relative invasion efficiency into *Ank-1*$^{(MRI96570/+)}$ and *Ank-1*$^{(MRI95845/MRI95845)}$ erythrocytes was examined through IVET assay, where parasitaemia ratio was calculated from parasite load of either *Ank-1*$^{(MRI96570/+)}$ to wild-type (a), *Ank-1*$^{(MRI95845/MRI95845)}$ to wild-type (b), or *Ank-1*$^{(MRI96570/+)}$ to *Ank-1*$^{(MRI95845/MRI95845)}$ erythrocytes (c) (n=5-7). The parasite growth inhibition was determined via TUNEL assay on infected RBCs (DAPI-positive) as an indicator of apoptotic and necrotic parasites (d). The proportion of TUNEL-positive infected RBCs was counted for *Ank-1*$^{(MRI96570/+)}$, *Ank-1*$^{(MRI95845/+)}$ and *Ank-1*$^{(MRI95845/MRI95845)}$ mice at 1-5% parasitaemia at ring stage (6-8 hours) and late trophozoite (18-20 hours) stage (n=4)(e). *P<0.05, **P<0.01, ***P<0.001. Error bars indicates SEM.

Figure 4

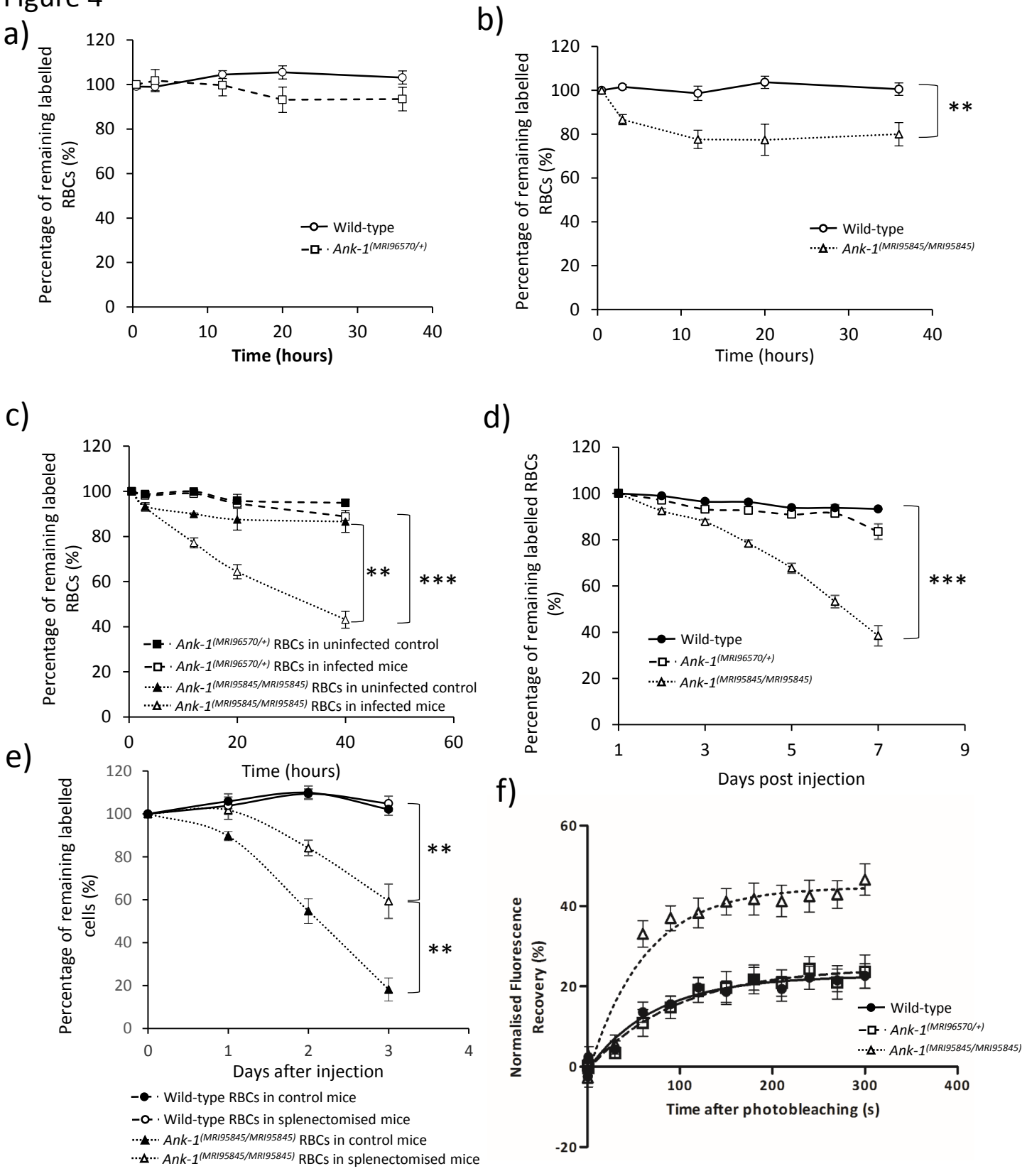

Figure 4. The clearance of wild-type, *Ank-1*$^{(MRI96570/+)}$ *Ank-1*$^{(MRI95845/MRI95845)}$ erythrocytes during malaria infection and the mobility of erythrocytic Band 3. The remaining percentage of labelled RBCs was monitored during the course of IVET assays, comparing between wild-type and *Ank-1*$^{(MRI96570/+)}$ erythrocytes (a), wild-type and *Ank-1*$^{(MRI95845/MRI95845)}$ erythrocytes (b), and *Ank-1*$^{(MRI96570/+)}$ and *Ank-1*$^{(MRI95845/MRI95845)}$ erythrocytes (c) (n=5-7). The half-life of wild-type, *Ank-1*$^{(MRI96570/+)}$ *Ank-1*$^{(MRI95845/MRI95845)}$ erythrocytes during malaria infection as determined by biotinylation of RBCs when parasites were detectable (n=6-7) (d). The clearance of), wild-type and *Ank-1*$^{(MRI95845/MRI95845)}$ erythrocytes in splenectomised and non-splenectomised mice infected with *P. chabaudi* over 3 days starting from 1% parasitemia (n=6) (e). The band 3 mobility on RBC membrane was measured using Fluorescence recovery after Photobleaching (FRAP), showing the recovery rate of fluorescence as a result of Band 3 migration to the bleach spot (n=9-21) (f). ** P<0.01, *** P<0.001. Error bars indicate SEM.

Supplementary figures

S1 Table

S1 Table. The candidate genes for MRI96570 and MRI95845 mutations.

a)

Chromosome	Gene name	Location	Reference base	Variant base	Number of mutant mice with mutation	LOD score (Threshold: 1.9)
3	*Fat4*	38888347	T	A	0/10	-2.81
7	*Rhcg*	79601661	T	C	0/10	-2.81
8	*Ank1*	23119400	T	A	10/10	2.81
X	*Plxnb3*	73763183	G	T	0/10	-2.81

b)

Chromosome	Gene name	Location	Reference base	Variant base	Number of mutant mice with mutation	LOD score (Threshold: 2.0)
8	*Ank1*	23085597	T	A	10/10	2.81
8	*Pnpla6*	3531116	G	A	8/10	1.24
9	*Zglp1*	21062907	G	A	0/10	-2.81
16	*Snai2*	14708259	A	C	0/10	-2.81
16	*Tbc1d23*	57191544	T	C	0/10	-2.81

Variants from exome sequencing were filtered to exclude strain-specific variants and variants found in other ENU-induced mice. Variants that were shared between the two mice carrying MRI96570 mutation or MRI95845 mutation are shown in (a) and (b), respectively. For each mutation, the candidate genes were Sanger sequenced in affected mice to determine the correlation between the genetic mutations and the phenotype by calculating the LOD score. LOD Threshold = 1.9 for MRI96570, 2.0 for MRI95845 (n= 10).

S1 Figure

a)

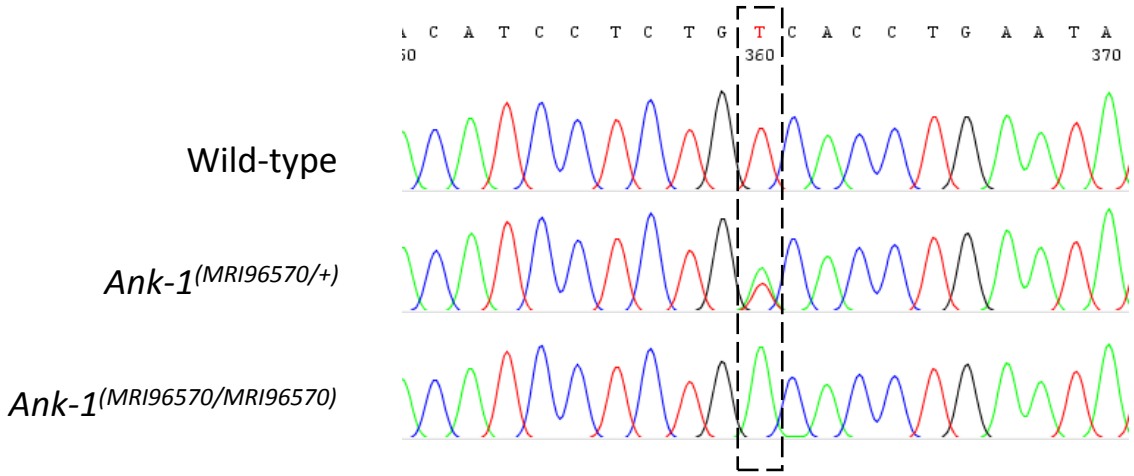

b)

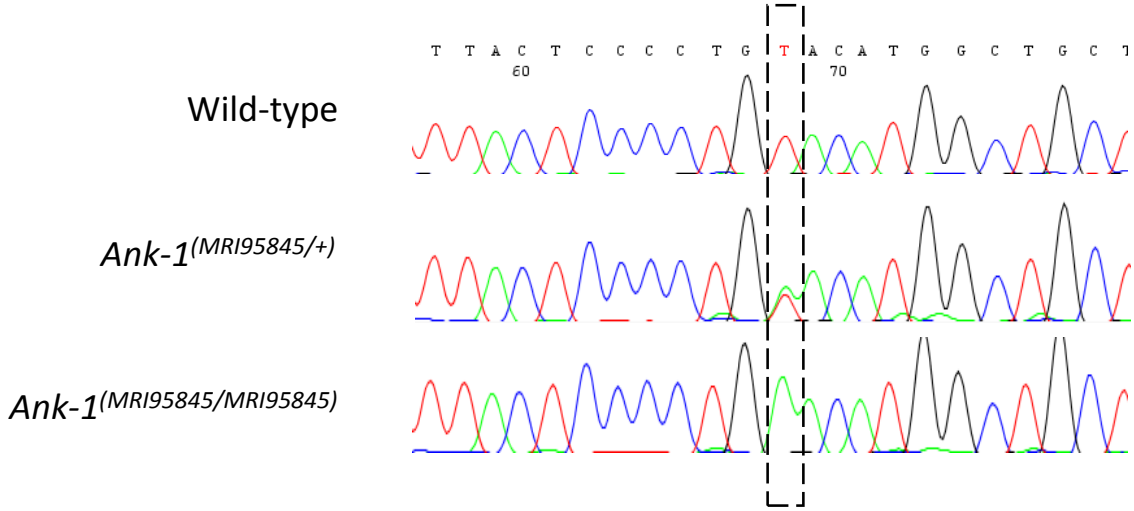

S1 Figure. The location of *Ank-1*$^{(MRI96570)}$ and *Ank-1*$^{(MRI95845)}$ mutation. Sanger sequencing of mice carrying *Ank-1*$^{(MRI96570)}$ revealed a T to A transversion in exon 34 of *Ank-1* gene, which is predicted to induce a premature stop codon (a). Mice carrying *Ank-1*$^{(MRI95845)}$ mutation were found to have a T to A transversion in exon 5 of *Ank-1* gene, which is predicted to cause a missense mutation from tyrosine to asparagine at residue 149 (b).

S2 Table. The complete blood count of *Ank-1*$^{(MRI96570/+)}$, *Ank-1*$^{(MRI95845/+)}$ and *Ank-1*$^{(MRI95845/MRI95845)}$ mice.

	Wild type	*Ank-1*$^{(MRI96570/+)}$	*Ank-1*$^{(MRI95845/+)}$	*Ank-1*$^{(MRI95845/MRI95845)}$
WBC (x10^6 /ml)	11.3±0.3	11.2±0.4	11.9±0.8	12.1±0.8
RBC (x10^9 /ml)	10.1±0.1	11.0±0.1***	10.7±0.1***	10.9±0.1***
HGB (g/L)	150.5±0.8	150.7±1.1	148.8±1.9	142.6±1.7*
MCV (fL)	52.3±0.2	46.9±0.2***	46.6±0.2***	43.0±0.1*** ^
MCH (pg)	14.9±0.1	13.7±0.1***	13.9±0.1***	13.1±0.2*** ^
MCHC (g/L)	285.3±1.2	290.3±1.8	298.3±2.4	294.7±4.0
RDW (%)	14.5±0.1	15.3±0.1***	16.1±0.3***	18.4±0.2*** ^
PLT (x10^6 /ml)	1036±31	1051±34	992±51	1026±53
Retics (%)	2.23±0.26	3.34±0.42	3.33±0.46	5.68±0.43***

The blood parameters were obtained from a haematological analyser ADVIA 120. WBC = white blood cell count; RBC = red blood cell count; HGB = total haemoglobin; MCV = mean corpuscular volume; MCH = mean corpuscular haemoglobin; MCHC = mean corpuscular haemoglobin concentration; RDW = red cell distribution width; PLT = platelet counts; Retics = percentage of reticulocytes, n=23-50. Bonferroni adjusted significance threshold = 0.001852, * P< 0.001, ** P< 1x10^{-5} compared to wild-type mice; whereas ^ P<0.001 compared to *Ank-1*$^{(MRI95845/+)}$ mice.

S2 Figure

a)

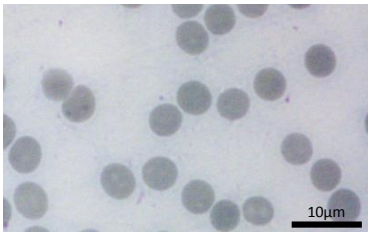

Wild-type

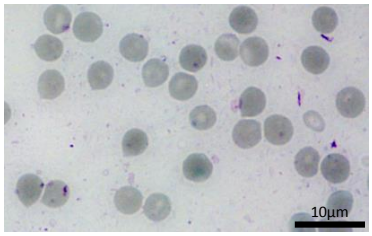

Ank-1$^{(MRI96570/+)}$

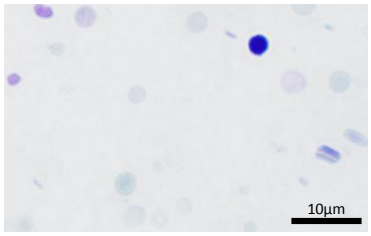

Ank-1$^{(MRI96570/MRI96570)}$

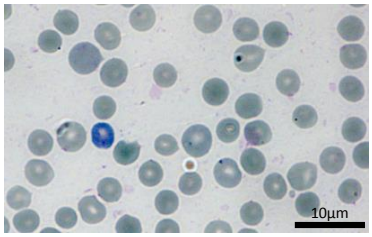

Ank-1$^{(MRI95845/+)}$

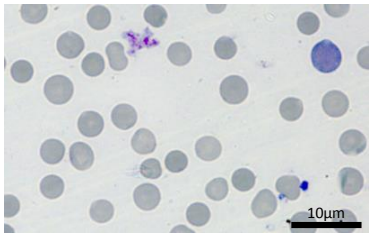

Ank-1$^{(MRI95845/MRI95845)}$

b)

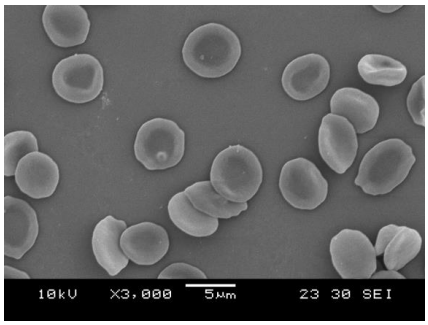

Wild-type

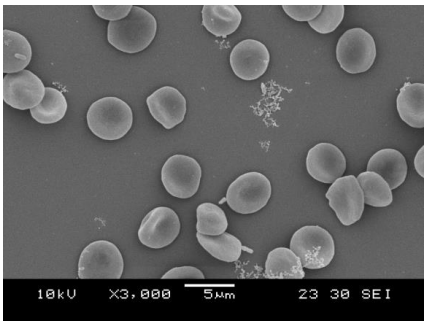

Ank-1$^{(MRI96570/+)}$

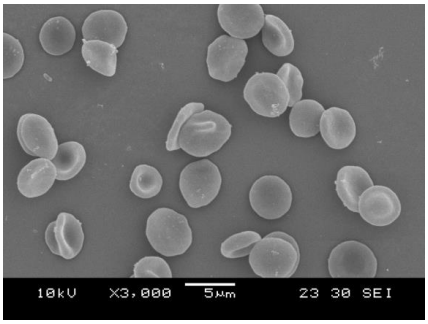

Ank-1$^{(MRI95845/+)}$

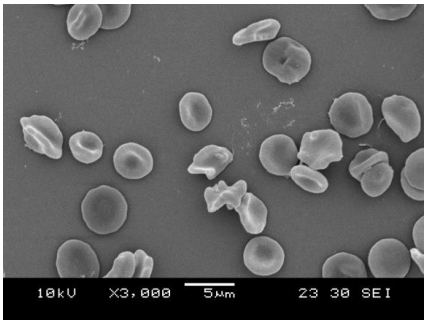

Ank-1$^{(MRI95845/MRI95845)}$

S2 Figure. The RBC morphology of mice carrying *Ank-1*$^{(MRI96570)}$ or *Ank-1*$^{(MRI95845)}$ mutation. Giemsa-stained blood smears as examined under light microscope at 1000x magnification (a). Scanning electron microscopic images showing the RBC shape of *Ank-1*$^{(MRI96570/+)}$, *Ank-1*$^{(MRI95845/+)}$ and *Ank-1*$^{(MRI95845/MRI95845)}$ mice (b).

S3 Figure

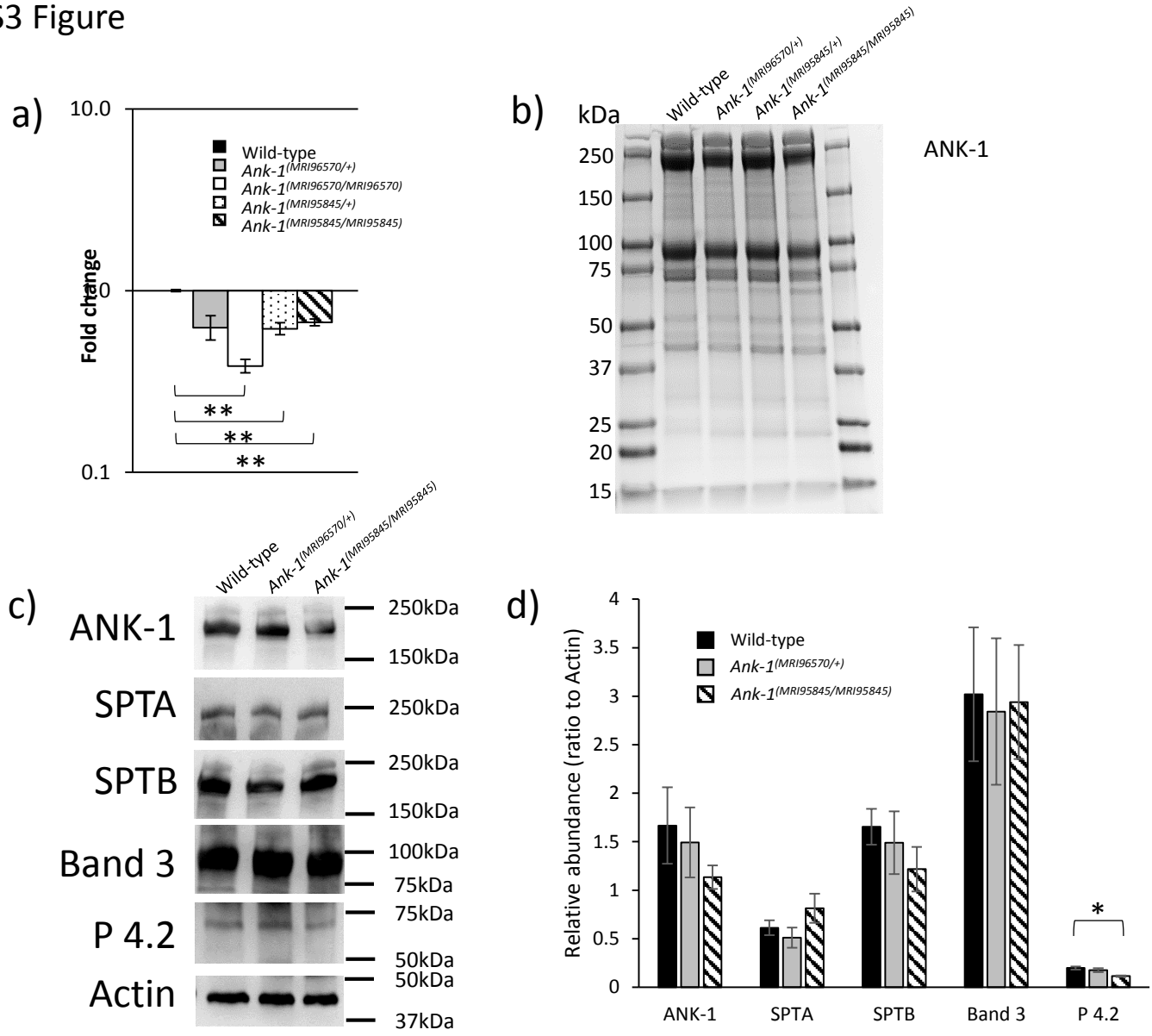

S3 Figure. The expression of *Ank-1* and other RBC cytoskeletal proteins in mice carrying *Ank-1*$^{(MRI96570)}$ or *Ank-1*$^{(MRI95845)}$ mutation. Quantitative PCR was carried out on E14 embryonic livers to examine *Ank-1* expression levels (n=3) (a). The abundance of ANK-1 and other RBC cytoskeletal protein levels of of *Ank-1*$^{(MRI96570/+)}$, *Ank-1*$^{(MRI95845/+)}$ and *Ank-1*$^{(MRI95845/MRI95845)}$ mice as examined via Coomassie (b) and Western blot (c) on membrane of mature RBCs. The relative abundance of various cytoskeletal protein levels calculated from western blots (n=3) (d). SPTA = α-spectrin, SPTB = β-spectrin, P 4.2 = Protein 4.2. * P<0.05, ** P<0.01. Error bars indicate SEM.

S4 Figure

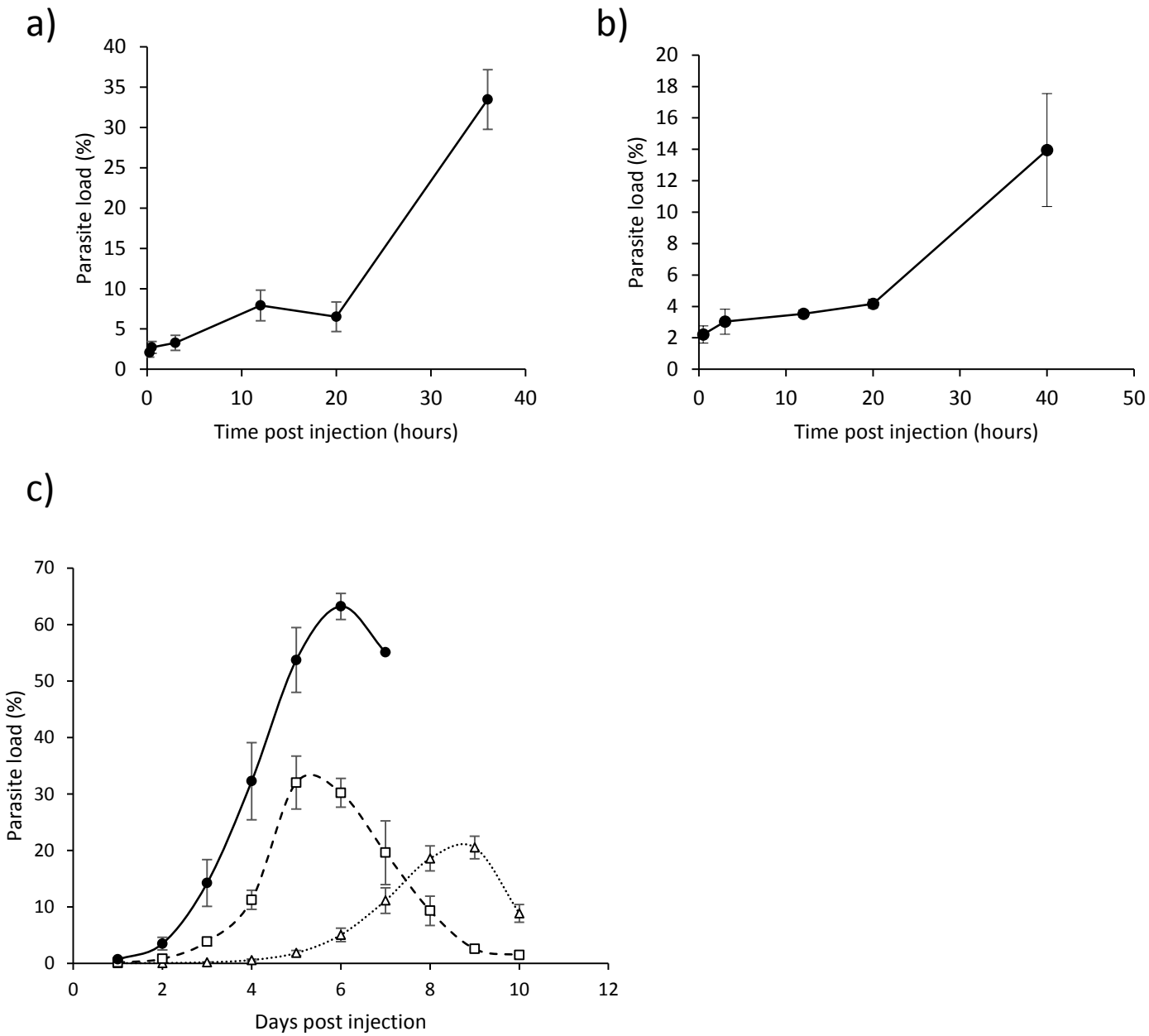

S4 Figure. The parasitaemia of the host mice during IVET assays and half-life assay. The parasitaemia curve of the host mice during IVET assays, when comparing wild-type with *Ank-1*$^{(MRI95845/MRI95845)}$ erythrocytes (a), and *Ank-1*$^{(MRI96570/+)}$ with *Ank-1*$^{(MRI95845/MRI95845)}$ erythrocytes (b) (n=5-7). The parasitaemia curve of wild-type, *Ank-1*$^{(MRI96570/+)}$ and *Ank-1*$^{(MRI95845/MRI95845)}$ mice during RBC half-life assay (n=6-7) (c).